Influence of polymer polarity and association strength on the properties of poly(alkyl ether) based supramolecular melts

Ana Rita Brás[1], Ana Arizaga[1], Daria Sokolova[1,2], Uxue Agirre[1], Maria Teresa Viciosa[3,4], Aurel Radulescu[5], Sylvain François Prévost[6], Margarita Kruteva[7], Wim Pyckhout-Hintzen[7], Annette Monika Schmidt[1]*

[1]Institute of Physical Chemistry, University of Cologne, 50939 Cologne, Germany

[2]Chemistry Department, University of Basel, BPR 1096/ 4058 Basel, Schweiz

[3]IN – Institute of Nanoscience and Nanotechnology, Instituto Superior Técnico, University of Lisbon, Avenida Rovisco Pais, 1049-001 Lisbon, Portugal

[4]Centro de Química Estrutural, Complexo I, Instituto Superior Técnico, University of Lisbon, Avenida Rovisco Pais, 1049-001 Lisbon, Portugal

[5]Jülich Centre for Neutron Science (JCNS-1), Forschungszentrum Jülich GmbH, 52428 Jülich, Germany

[6]Institut Laue-Langevin, 71 Avenue des Martyrs, CS 20156, 38042 Grenoble Cedex 9, France

[7]Jülich Centre for Neutron Science (JCNS-1), Forschungszentrum Jülich GmbH, 52428 Jülich, Germany

KEYWORDS: supramolecular polymers; poly (ethylene oxide), poly (propylene oxide), thymine-1-acetic acid; diaminotriazine; 2-ureido-4[1H]-pyrimidinone; homocomplementary; heterocomplementary; hydrogen bonding, polarity, bond lifetime, segmental dynamics

ABSTRACT: The present work focuses on the impact of polymer polarity and hydrogen-bonding (H-bonding) end groups association strength on the structure and dynamics of poly(alkyl ether) based supramolecular model polymers studied by means of small angle scattering (SAS), rheology, broadband dielectric spectroscopy (BDS) and differential scanning calorimetry (DSC). These consist of poly (propylene oxide) (PPO) or poly (ethylene oxide) (PEO) backbone that self-assembly in the bulk via hydrogen bonding (H-bonding). Diaminotriazine (DAT) and thymine-1-acetic acid (THY), as well as 2-ureido-4[1H]-pyrimidinone (UPY) are the H-bonding end groups of choice. Both PPO and PEO bearing either DAT or THY as end groups associate into linear chains, but PPO-THY/DAT forms longer chains in comparison with PEO-THY/DAT. The lower polarity of the backbone results in stronger associations for the same end groups. However, the temperature dependence of the association/dissociation lifetimes for this H-bonding type is independent of the different main chain polarity as these breaking times do not exceed the rouse chain dynamics as expected within the Cates model. PPO-UPY forms a transient network characterized by the interplay between small transient bonds controlled by the characteristic times of association/dissociation between pairs of UPY groups involving probably just two ends, revealed by the similar dielectric spectra with PPO backbone, and a more stable bond type of

associate that forms phase separated UPY clusters. The latter are responsible for the physical crosslinks in the network and result in the rubbery-like plateau of the rheological spectra. PPO-UPY has similar structure to PEO-UPY, as validated by small angle scattering, but the UPY detachment times in the clusters are higher for PEO-UPY than for PPO-UPY, though the activation energies are very close and match the typical energy barrier specifically imposed by the hydrogen bonds. Moreover, while the segmental relaxation times and the glass transition temperature (T_g) of PPO-UPY is similar to PPO, PEO-UPY has the highest T_g value and a much slower segmental relaxation as compared to PEO and PPO based supramolecular polymers. This seems to indicate that the H-bonding association dynamics of the UPY groups is strongly influenced by the main chain polarity that play a fundamental role in defining the time scale of the association process.

1. INTRODUCTION

A prominent topic in polymer chemistry over the past years has been the development of new polymers called supramolecular that possesses dynamic supramolecular bonds instead of permanent covalent bonds. The character of these dynamic interactions, which can be hydrogen bonds, metal complexes, or π/π stacking, enables fascinating applications such as stimuli-responsive materials[1–3] and self-healing polymers.[4–8] These applications usually involve their mechanical and viscoelastic properties, which can be tuned by modifying the supramolecular bonds associating strength and morphology, the polymer architecture and the main chain polarity.[9–13] Typically, dynamic bonds that are generated in the melt can behave like permanent bonds and form a network, e.g., at low temperature. Thus, even relatively weak dynamic bonds, like hydrogen bonds can display significant effects in the melt.[14–17] In this context, knowledge of the dynamic

supramolecular structure and the time scales of formation of the supramolecular organization is crucial for the understanding of the influence of the main chain polymer polarity and thermodynamic interactions on the properties of the supramolecular system.

A fundamental study of the role of different H-bonding association strength on the structure and the dynamics of bifunctional poly(ethylene oxide) (PEO) in the bulk by using heterocomplementary hydrogen-bonding end groups (THY and DAT) on the one hand, homocomplementary self-assembly moieties (UPY) on the other hand, has been recently studied by some of us.[18] It is shown that the different H-bonding types have a strong impact on the morphology and the tendency to phase separate and are of influence both on the segmental and the H-bonding association dynamics of the supramolecular polymer.[18] In fact, the heterocomplementary H-bonding end-groups (THY and DAT) have also been attached to other polymers such as bifuctional polyisobutylene (PIB) and poly(n-butyl acrylate) (PnBAs) polymers.[13,19,20] These supramolecular polymers either form a linear, and entangled supramolecular polymer chains or a phase segregated, cluster network-like system. While these differences seem to be related with the diverse nature of the backbone chain polarity on the structure and dynamics of these bifunctional hydrogen bonded supramolecular polymers, a systematic study of the exact role of the polarity on the formation of supramolecular networks and on the segmental dynamics and H-bonding association in telechelic polymers is rather limited to date.

Polypropylene oxide (PPO) is a poly(alkyl ether) showing similarity but with lower polarity than PEO and has been largely studied by different techniques in the last decades.[12,21–27] It is a so-called "type A" polymer, feature an electrical dipole moment formed along the backbone chain contour, so that it is possible to study the segmental relaxation and the normal modes easily via dielectric spectroscopy.[28,29] The segmental motion responsible for the α- relaxation is regarded as local and

should cover only few repeating units, but the so-called normal mode process is highly cooperative and involves the whole polymer chain.[29] While in the past the association of heterocomplementary bifunctional PPO, bearing also either DAT or THY as end groups, was studied by small-angle neutron scattering (SANS), the dynamics of such supramolecular polymers has not been addressed in any detail, in particular the segmental and association dynamics. The same happens for the homocomplementary bifunctional PPO having at the ends UPY groups.

Therefore, here we aim to understand: i) the influence of two types of H-bonding end groups with different association strength and ii) the role of the bifunctional defined poly(alkyl ether), PEO and PPO, backbone main chain polymers that differ on the number of methyl groups and polarity, and have the same H-bonding groups at the ends on the structural and dynamic phenomena of these two poly(alkyl ether) based model supramolecular polymers. In this context, we present a combined study of small angle scattering, linear rheology, broadband dielectric spectroscopy and differential scanning calorimetry, to unravel the differences on the microscopic structure, H-bonding association and segmental dynamics and consequently on the underlying rheological macroscopical mechanisms of bifunctional supramolecular PEO and PPO based polymers. By comparing polymers with different backbone polarity and H-bonding association strength, we present a consistent interpretation of the data and discuss the parameters that play a key role on their different structural and dynamical behavior.

2. EXPERIMENTAL SECTION

2.1 Samples

Bifunctional THY-telechelic PPO (PPO-THY), bifunctional DAT- telechelic PPO (PPO-DAT) and bifunctional UPY-telechelic PPO (PPO-UPY) are synthesized from dihydroxy PPO (PPO-

OH) according to procedures in the literature.[8,29–32] The synthetic details of the polymer functionalisation and the characterization of the products are presented in the Supporting Information (S.I.). **Table 1** repeats, in short, the results. For all polymers, ^{1}H nuclear magnetic resonance (NMR) is used to determine the number average molar mass (M_n) and the functionalization degree (f) and size exclusion chromatography (SEC) is used to determine the polydispersity index (PDI). The number of repeating monomer units, N, is for all polymers the same as for the reference PPO polymer (from which the supramolecular polymers are synthesized), $N = 35$, which results from $M_n = N \cdot M_0$ with $M_n = 2047$ g·mol^{-1}, the molar mass of one PPO polymer unit and M_0 = 58 g·mol^{-1}, being the molar mass of one PPO monomer.

The equimolar mixture (50:50) of bifunctional PPO-THY and PPO-DAT compounds are prepared by solution blending in chloroform and dried under high vacuum conditions for two days. The structure of both THY and DAT hetero-complementary association as well as UPY homo-complementary association is illustrated in **Figure 1**.

Table 1. Characteristics of the supramolecular polymers and the reference PPO polymer: M_n is the molar mass of one polymer unit, PDI is the polydispersity index and f is the functionalization degree of the supramolecular polymer blocks.

	PPO	PPO-THY	PPO-DAT	PPO-UPY
M_n (^{1}H NMR)	2047	2320	2200	2550
PDI (SEC)	1.05	1.06	1.06	n.d.
f(^{1}H NMR)*	-	99%	99%	95%

*The uncertainty associated to the values is within 1%-2%.

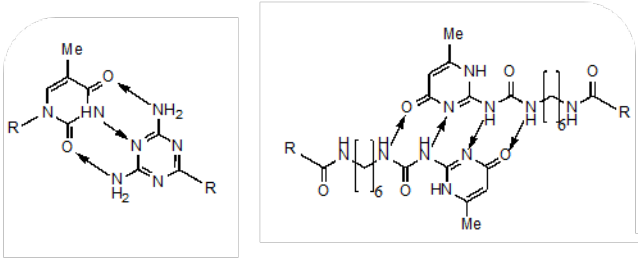

a) THY/DAT hetero-association

b) UPY homo-association

Figure 1. Hydrogen bonds involved in a) THY/DAT hetero-complementary association and in b) UPY homo-complementary association end groups.

2.2. Nuclear Magnetic Resonance (NMR)

^{1}H NMR spectroscopy of the studied polymers is performed using a Bruker DPX 300 (300.13 MHz) either in $CDCl_3$ or DMSO-d6 at ambient temperature. As an internal standard, the solvent signal is set to 7.26 ppm or 2.50 ppm, respectively. The chemical shift is assigned in ppm.

2.3. Size Exclusion Chromatography (SEC)

SEC is performed with tetrahydrofuran (THF) as the eluent on a SEC system from hs GmbH, Germany, with the following components: pump (intelligent pump Al-12, Flow), degasser (Gastorr AG-32, Flow), autosampler (S5250, Sykam, Eresing, Germany), RI detector (RI2012–A, Schambeck, Bad Honnef, Germany), UV detector (S3245 UV/Vis-detector, Sykam, Eresing, Germany) and column system (pre-column with 100 Å pore size and three columns of 10,000 Å, 1000 Å and 100 Å, respectively) from MZ Analysentechnik; Germany with MZ-Gel SD plus as the stationary phase. Polystyrene standards (Polymer Laboratories) in the molar mass range of M_n = 925 g·mol^{-1} to 1.98 × 10^6 g·mol^{-1} are used for the calibration of the system.

2.4. Small Angle Scattering

SANS measurements are performed both at the SANS diffractometer KWS2@FRM2, Munich, Germany and on the instrument D11 at the Institut Laue-Langevin (ILL) in Grenoble, France. At the KWS2 the absolute scattering intensities are measured over a scattering range from $Q = 0.0047$ Å^{-1} to 0.44 Å^{-1} using sample-to-detector distances of 2 m, 4 m, and 8 m and corresponding collimation lengths and at the D11 a Q range of 0.0020 Å^{-1}–0.50 Å^{-1} is covered using also three different configurations with a wavelength of λ = 6.0 Å (full width at half-maximum (FWHM) 9%), sample-to-detector (SD) distances of 1.4 m, 8 m, and 39 m, and collimations of 10.5 m, 8 m, and 40 m, respectively. All data are reduced using in-house software, correcting measured intensities for the transmission, dead-time, detector background (with boron carbide as a neutron absorber at the sample position), sample background (empty cell), and the absolute scale (obtained from a tabulated value of a 1.5 mm sheet of plexiglas). Samples were measured at 333 K in 1 mm thick quartz cuvettes (QX, Hellma). The incoherent background caused mainly by protons in the sample is determined at a high scattering angle, set as a constant and subtracted from the data.

Small angle X-ray scattering (SAXS) data are measured at the GALAXI diffractometer based in the institute JCNS-2 at Forschungsszentrum Jülich.[33] The X-ray source utilizes a liquid metal jet target of a GaInSn alloy as the anode to which 70 keV electrons are sent. The resulting X-rays are monochromatized to allow only Ga K-α radiation with a photon energy E = 9.243 keV to pass to obtain a wavelength λ = 1.34 Å. Two four-segment slits that are separated by 4 m distance collimate the beam and confine the size to about (0.7×0.7) mm^2. A third slit reduces the scattering from the edges of the second one. A sample-to-detector distance of 80 cm calibrated using Bragg reflections from silver behenate resulting in a Q range of 0.05 Å^{-1}– 0.7 Å^{-1} is used. Absolute intensities in (cm^{-1}) are obtained by the calibration with a secondary standard, consisting of a hexafluoro-ethylene-propylene copolymer (Dupont). The measured polymers are sealed in

borosilicate capillaries of 2 mm nominal inner diameter and placed in the vacuum chamber at an experimental temperature of 333 K. Standard corrections for cell scattering and detector efficiency is performed.

2.5. Rheology

Rheological measurements are performed using an AR-G2 rheometer (TA Instruments, New Castle, DE, USA) with a plate-plate geometry (20 mm) in which approx. 0.5 g of sample is used. The gap between the plates is 1 mm. Strain sweep experiments are performed at a frequency of 1 Hz in the strain regime $0.001 < \gamma < 0.5$. Frequency sweep experiments in the range of 0.1 Hz – 100 Hz are carried out in the linear viscoelastic regime. From these measurements, the frequency dependent storage modulus G', and loss modulus G'' for PPO-THY/DAT is determined at 278 K, 298 K, 318 K, 338 K and 358 K and for PPO-UPY at 283 K to 363 K in steps of 10 K. Steady shear viscosities in the shear rate range $0.01\ s^{-1} < \dot{\gamma} < 500\ s^{-1}$ are measured for PPO-THY/DAT at and for PPO-UPY at the same temperatures as for the strain sweep measurements. The temperature stability, ΔT for all measurements is < 0.05 K.

2.6. Differential Scanning Calorimetry

Differential scanning calorimetry (DSC) measurements are performed in standard sealed aluminum containers using a heat-flux calorimeter DSC-1 (Mettler Toledo) and a DSC Q2000 from TA Instruments Inc. (Tzero DSC technology) operating in the heat flow T4P option. Measurements were carried out under anhydrous high purity nitrogen at flow rate of 50 mL/min. All polymers are submitted to two cooling and two heating runs between 193 K and 373 K recorded at a rate of 10 $K.min^{-1}$ The glass transition temperature T_g is determined in the 2nd heating cycle as the temperature of the onset of the heat capacity increment in the transition, using the step-analysis-tool implemented in the instrument evaluation software.

2.7. Dielectric Relaxation Spectroscopy

To determine the isothermal dielectric behavior, characterized by the complex dielectric permittivity $\varepsilon^*(\omega) = \varepsilon'(\omega) - i\varepsilon''(\omega)$ (ω, angular frequency; ε', real part; ε'', imaginary part; $i = -1^{1/2}$), dielectric relaxation spectroscopy (DRS) measurements are conducted with an Alpha-A impedance analyzer connected to a Quatro Cryosystem temperature controller (both from Novocontrol), in a frequency range from 10^{-1} Hz – 10^6 Hz, measured on heating from 153 K to 313 K every 2 degrees. Thermalized in a dry nitrogen flow, the maximum permitted deviation in temperature is 0.2 K. All samples are measured in a capacitor composed of two gold-plated electrodes of 20 mm diameter separated by two silica spacers of 49 μm thickness, which yields a capacitance of ~ 20 pF for the empty cell; further details on this type of cell can be found elsewhere.[34,35]

3. RESULTS AND DISCUSSION

In the following both the structure and dynamics of PPO-THY/DAT and PPO-UPY are studied and compared by means of small angle scattering and rheology, DRS and DSC, respectively. This way the influence of the different H-bonding association types on the PPO backbone block is revealed. Indeed THY/DAT association is of hetero-complementary type, while UPY association is a homo-complementary one. This study is then followed by a comparison with the structure and dynamics of supramolecular PEO-THY/DAT and PEO-UPY published recently.[18] By comparing the different polymer backbones blocks functionalized with the same H-bonding end groups and presenting a consistent interpretation of the data we learn also which parameters, either the main chain polymer polarity or the polymer segmental dynamics, either the H-bonding association

dynamics play the key role on the different structural and dynamical behavior of these supramolecular polymers type.

3.1. Structure

In this section, the analysis of the morphology of supramolecular PPO-THY/DAT and PPO-UPY in the melt is presented.

The structural parameters of a PPO polymer that consist of the backbone block of our supramolecular polymers (**Table 1**), and considering the theoretical definitions for a random walk model in an ideal Gaussian polymer chain in the melt (equation S11 used in the random phase approximation (RPA) theory description at point II in the S.I.), are the following [36–41]: end-to-end distance, $R_{\mathrm{e}} = 35$ Å, radius of gyration, $R_{\mathrm{g}} = 14$ Å, the statistical segment length $l_{\mathrm{st}} \approx 6$ Å, the Kuhn length $b = 8.0$ Å and the number of Kuhn segments $N_{\mathrm{K}} = 19$.[36,40,41] These parameters are used to check and confirm the theoretical model approaches employed to describe PPO-THY/DAT and PPO-UPY scattering experimental data.

Supramolecular PPO-THY/DAT

The structure of the equimolar (50:50) mixture of bifunctional PPO-THY/DAT is investigated in the melt by SAXS. **Figure 2** shows the SAXS results for a fully hydrogenated PPO-THY/DAT at different temperatures, i.e. intensity $I(Q)$ versus scattering vector Q. The contrast is given by the electron density difference of the PPO backbone polymer block vs. the H-bonding end groups, and the scattering data is corrected by the subtraction of the scattering data contribution of the PPO polymer. The as such corrected intensities indicate a clear correlation hole peak typical for a block copolymer observed at intermediate Q roughly ~ 0.18 Å^{-1}.[13,40] This corresponds approximately to a distance of 34.9 Å, which is the end-to-end distance R_{e} of a Gaussian chain of our PPO backbone polymer block ($R_{\mathrm{e}} = 35$ Å). The height of the correlation peak decreases with increasing

temperature and it is given by the number of correlated blocks (N_{assc}), the scattering length densities (ρ), and the Flory-Huggins parameters (χ).[29,30,42] At high Q, the curve shows the same typical Q^{-2} behavior of random walk chain statistics, where the identity of the backbone polymer blocks structure is lost. The Q^{-2} behavior is an undeniable characteristic of the polymer morphology and therefore rules out any more compact, segregated morphologies or structure factor-related Bragg peak from a characteristic distance between scattering particles. At the lowest Q, a parasitic scattering contribution following a Q^{-4} power law is observed, but since it is assigned to electron deficient voids or dust in the glass-sealed capillaries, no information can be obtained regarding the morphology and it is not considered here. Therefore, only for stability purposes in the fitting process, the respective background is modelled by a polynomial function up to Q^{-3} following a procedure suggested by Vonk.[43]

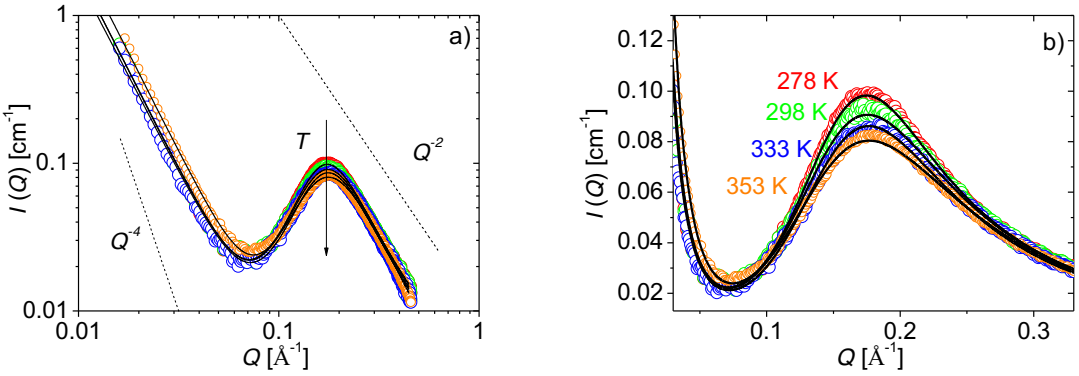

Figure 2. a) SAXS data for PPO-THY/DAT at T = 278 K (red); T = 298 K (green); T = 333 K (blue) and T = 353 K (orange). The black lines correspond to the fit to the SAXS data with the modified RPA model. The dashed black lines demonstrate distinct Q power law dependencies, $I(Q) \propto Q\text{^}(P)$, with $P = -2$ or -4. b) Zoom to the SAXS data of the correlation peak region for PPO-THY/DAT at the same temperatures as in a).

The observation of a block copolymer-like scattering signal on supramolecular polymers requires the use of random phase approximation (RPA) formalism for multicomponent systems as has already been shown in literature[29,30,42] (more details can be also found in the S.I.):

$$\frac{I(Q)}{\Delta\varrho^2} = \frac{S^0_{\mathrm{AA}}S^0_{\mathrm{BB}} - S^{0^2}_{\mathrm{AB}}}{(S^0_{\mathrm{AA}} + S^0_{\mathrm{BB}} + 2S^0_{\mathrm{AB}}) - 2\frac{\chi_{\mathrm{AB}}}{\sqrt{\nu_{\mathrm{A}}\nu_{\mathrm{B}}}}\left(S^0_{\mathrm{AA}}S^0_{\mathrm{BB}} + S^{0^2}_{\mathrm{AB}}\right)} \quad (1)$$

In this work, we consider the binary system of a multiblock copolymer, as A block being the PPO backbone polymer chain and B block representing both THY/DAT associating end groups into a single effective block[29]. Thereby the system can be modelled as the general multiblock copolymer as $(\mathrm{AB})_{\mathrm{X}}$ copolymer with an association number *X* of the diblock units, representing the number of associated building blocks N_{assc}. This can be compared to the mass-averaged polymerization degree $\langle N_{\mathrm{assc}}\rangle_{\mathrm{w}}$ in polycondensation theory [30]. We have thus applied a full two-component RPA including the Flory-Huggins interaction parameter χ_{AB}. With the number of repeating monomer units denoted as N_{A} for the backbone polymer chain and N_{B} for the compound end groups, respectively, specific volumes v_{A}, and v_{B}, the interaction parameters polymer–end groups χ_{AB}, the contrast $\Delta\rho^2 = (\rho_{\mathrm{A}} - \rho_{\mathrm{B}})^2$and the number of associated building blocks N_{assc}. The ideal noninteracting structure factors, $S^0_{\mathrm{AA}}, S^0_{\mathrm{BB}}, S^0_{\mathrm{AB}}$ are given in function of the dimensionless parameter $a = (Q^2 \cdot l^2_{\mathrm{st}})/6$ such that $R^2_{\mathrm{g}} = aN$, where N is the specified "block length": equivalent to $N_{\mathrm{A}} = N = 35$ (in the case of reference PPO polymer) that is the number of repeating PPO monomer units of the backbone polymer block) and equivalent to $N_B = 3$ repeating PPO monomer units (in the case of THY/DAT block) and reflecting the random-walk statistics of the building blocks, with l_{st} the effective statistical segment length of the Gaussian subchains resulting from the approximation including the end groups into the more flexible building blocks. More details on the RPA model can be found in the Supporting Information and in [29] and [30].

In this context, the only parameters adjusted during the fit procedure are N_{assc}, l_{st} and χ_{AB} , as all other parameters are known and kept constant, such $N_{\mathrm{A}} = N = 35,\ N_{\mathrm{B}} = 3$, contrast $\Delta\rho^2 = (\rho_{\mathrm{A}} - \rho_{\mathrm{B}})^2$ and volumes (these numbers are given in section II and III of the S.I.). The black lines in **Figure 2** display the resulting fits to the SAXS data using the modified RPA model. The statistical segment length, l_{st} determined for all temperatures is in average 7.5 Å, larger than for the unfunctionalized PPO ($l_{\mathrm{st}} = 6$ Å) as it absorbs the different rigidities of the blocks.[44,45] The derived χ_{AB} ($\chi_{\mathrm{PPO-THY/DAT}}$) interaction parameter is relatively insensitive to the temperature with values of 3.3- 3.9 in agreement to the theoretical estimations (present in section III of the S.I.)[29,46]. The fit also yields a number of associated blocks, N_{assc}, which as expected decreases with increasing temperature, from $N_{\mathrm{assc}} \approx 30$ at $T = 353$ K and $N_{\mathrm{assc}} \approx 500$ at $T = 278$ K. However, the sensitivity of the peak intensity to the degree of association is severely limited, as the position of the RPA peak becomes virtually independent for $\langle N_{\mathrm{assc}} \rangle_{\mathrm{w}} > 19$, therefore the obtained values cannot be considered as the absolute N_{assc}.[30] Nonetheless, it is clear that the association between THY and DAT end groups for PPO-THY/DAT at all measured temperatures results in longer polymer chains with a molar mass well above the entanglement molar mass of PPO-OH, $M_{\mathrm{e,PPO}} \approx$ 2800 g·mol^{-1}, which behave Gaussian-like and show random-walk behavior.

Supramolecular PPO-UPY

The structure of PPO-UPY is studied in the melt by both SAXS and SANS. **Figure 3** shows the obtained data for fully hydrogenated PPO-UPY at T = 333 K. The contrast is given by the electron density difference or by the scattering length density difference between the H-bonding UPY end groups and the backbone PPO polymer block, depending on the experiment source, either X-rays or neutrons, respectively. The PPO-UPY scattering data is corrected for background scattering by subtraction of the contribution of the PPO backbone polymer scattering data at the same

temperature. Qualitative observations from the as such corrected small angle scattering pattern show that on one hand the intermediate Q-range follows a power law, $I(Q) \propto Q^P$, with $P \sim -4$ and on the other hand an interaction peak can be spotted toward lower Q values, even though the scattering pattern is filled with high intensity. Both observations suggest that the morphology of this system consists of interacting compact structures due to phase segregation. Indeed the strong association between UPY end groups is largely favored as the estimated rather high value of Flory-Huggins interaction parameter, $\chi_{\mathrm{PPO-UPY}}$ points out (Section III of the S.I:).[13,19] Therefore, these compact structures should be composed by UPY end groups segregated in clusters separated by the PPO polymer chains, similarly to what is observed in colloidal and micellar systems.[47,48] Normally, these phase segregated structures are approximated to hard spherical cluster aggregates and are thus treated with the Percus–Yevick model.[36,49–51] The model assumes a suspension of hard spheres with repulsive interaction. The potential is infinite when two spheres touch each other. In the lowest Q-range a strong decay of the intensity following approximately a Q^{-3} power law is also evident; however, no relevant information can be obtained at this Q-range regarding the morphology. The scattering intensity per unit of volume for spherically symmetric particles as in the Percus-Yevick hard sphere model is well known and generally is written as:[41,52]

$$I(Q) = \phi \Delta\rho^2 V F(Q, R_\mathrm{c})^2 S(Q, R_\mathrm{d}) \qquad (2)$$

where ϕ is the volume fraction of particles, $\Delta\rho^2$ the contrast factor between PPO backbone polymer and UPY end group forming the spherical particles and V their volume. $P(Q, R_\mathrm{c}) = F(Q, R_\mathrm{c})^2$ is the form factor and $S(Q, R_\mathrm{d})$ the structure factor due to the contribution of the interactions between particles. Basically, the scattering intensity of the disordered particles can be attributed to the form factor of spheres with radius R_c (the spherical clusters) and the structure factor of hard spheres (the Percus-Yevick correlation radius due to the interactions between

spherical clusters) with a radius of R_d. We assume that the spherical particles are polydisperse. Therefore, the only parameters to be adjusted during the fit procedure are the mean sphere cluster radius R_c, the Percus–Yevick correlation radius of clusters R_d, the volume fraction of spherical clusters ϕ and the polydispersity σ, as all other parameters of the model are known such as the contrast factor $\Delta\rho^2$ and the volume. A detailed description of this viable model can be found in the Supporting Information and also in refs [36,49,52].

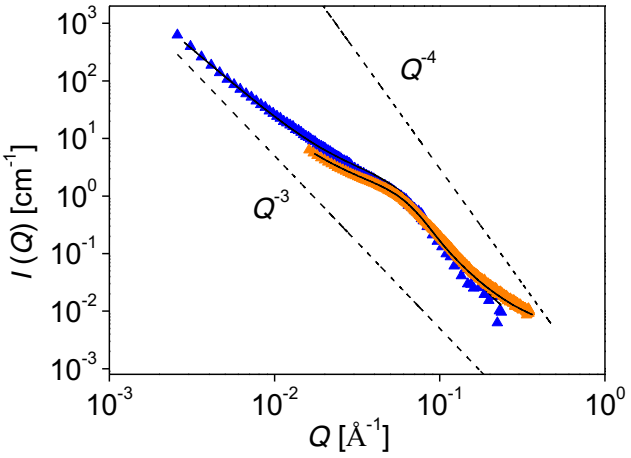

Figure 3. (a) Small angle scattering data of PPO-UPY at $T = 333$ K, blue triangles: SANS; orange triangles: SAXS. The black lines correspond to the fit to the data with the Percus–Yevick model. The dashed black lines demonstrate the distinct Q power law dependence, $I(Q) \propto Q^P$, with $P = -3$ or $P = -4$.

The black lines in **Figure 3** correspond to the fit to the data using the Percus–Yevick model. As displayed in **Figure 3**, a reasonable adjustment is obtained and, besides a slight difference at low Q values, both SAXS and SANS data is very similar for both measured temperatures. In fact, the values from R_d and R_c as $2R_d - 2R_c = 2 \times 43.1\text{Å} - 2 \times 24.7\text{Å} = 36.9$ Å and $2 \times 44.0\text{Å} - 2 \times 26.5\text{Å} = 34.9$ Å for both SAXS and SANS data, respectively at $T = 333$ K. correspond

approximately to the end-to-end distance of the PPO polymer ($R_e = 35$ Å). Moreover, the volume fractions in PPO-UPY ($\phi = 0.048$ and $\phi = 0.023$ for both SAXS and SANS, respectively) are relatively low and roughly agree with the calculated molar fraction of UPY end groups in the supramolecular polymer ($M_{n,UPY}/M_{n,PPO-UPY} = 0.06$). This is in accordance with the fact that highly attractive interactions decrease the critical volume concentration that depends sensitively on changes in the interaction between the aggregates or polydispersity, which here is ranging from ~37% to ~40%, for both SAXS and SANS, respectively. Still, this parameter is difficult to characterize as it depends greatly on the high Q scattering, whose range is relatively limited, especially for the SAXS data.[53] Added to this, the UPY aggregation number, N_{UPY}, defined as the number of UPY end groups per spherical cluster, is an important parameter to characterize the aggregates. From the fit parameter R_c, N_{UPY} can be calculated as $N_{UPY} = \frac{4\pi R_c^3 \rho N_A}{3M_{n,PPO-UPY}} = 15 - 18$ for SAXS and SANS respectively, as well as the molar density of elastically active strands ν_e given by $\nu_e = \frac{3\phi}{4\pi R_c^3 N_A}$=1.3 mol·m^{-3} and 1.0 mol·m^{-3} for both SAXS and SANS, respectively.[13,19] The density of the supramolecular polymer melt used is $\rho_{PPO-UPY} = 1.0$ g·cm^{-3}.[44] Taking into account the high interaction parameter between UPY groups and PPO backbone (see above) the results seem to be reasonable. It is demonstrated that PPO-UPY forms disordered spherical cluster aggregates as shown by the good agreement of the Percus–Yevick model to the data analysis. It is shown that UPY end groups are segregated in spherical clusters containing several of these groups.

Both structural analyses allow the conclusion that while PPO-THY/DAT associates into long linear chains, PPO-UPY forms disordered spherical cluster aggregates that are interconnected by PPO chains. Moreover, the Perkus-Yevick model fit to the data allows estimating the size and the volume fraction of the UPY spherical clusters and the number of UPY groups in the clusters.

3.2. Dynamics

The dynamics of both bifunctional supramolecular PPO polymers possessing at the ends both THY/DAT but also UPY is presented. As the dynamics of PPO backbone block polymer is amply developed,[30,54] here only a summary of the dynamic phenomena that are relevant for the understanding of the key differences between the different supramolecular PPO polymers is discussed.

3.2.1. *Differential Scanning Calorimetry*

The glass transition temperature (T_g) for all the studied systems is determined by DSC and the obtained values are presented in **Table 2**. The temperatures of the calorimetric glass transition are 204.8 K, 216.6 K and 208.2 K, respectively, for PPO, PPO-THY/DAT and PPO-UPY. The specific heat capacity, ΔC_p, of the calorimetric glass transition, are comparable in all systems, being equal to 0.64±0.02 J·(g·K)$^{-1}$, 0.47±0.02 J·(g·K)$^{-1}$and 0.67±0.02 J·(g·K)$^{-1}$ for PPO, PPO-THY/DAT and PPO-UPY, respectively. The T_g for PPO-THY/DAT increases almost 12 degrees in comparison with PPO backbone polymer block, consistent with the known increase in the glass transition temperature of linear associating polymers with intermolecular H-bonds [12,55]. This observation is in contrast to PPO-UPY, where no significant influence of chain end group association strength on T_g is found.[56]

Table 2. Calorimetric glass transition $T_{g,DSC}$ and the specific heat capacity, $\Delta C_p$for PPO polymer, PPO-THY/DAT and PPO-UPY.

	$T_{g,DSC}$ [K]*	ΔC_p [J·(g·K)$^{-1}$]
PPO	204.8	0.64
PPO-THY/DAT	216.6	0.47
PPO-UPY	208.2	0.67

*The uncertainties of the temperature are around ± 0.5 K, standard deviations from the mean independent determinations.

3.2.1. *Rheology*

Figure 4 presents the steady-shear viscosity measured as studied by rheology in the temperature range from 278 K to 358 K, with 20 K as temperature interval for PPO-THY/DAT and from 283 K to 363 K, in 10 K steps for PPO-UPY, respectively. While for PPO-THY/DAT the measured viscosity is independent of shear rate for all temperatures expected in the Newtonian regime,[57–59] under steady shear, PPO-UPY exhibits a shear thickening behavior at the lowest temperatures, as shown in **Figure 4a** and **b**, respectively. Shear thickening is characterized by an increase in effective viscosity when the shear rate increases past a certain critical value as evident in **Figure 4b** for $T = 283$ K and $T = 293$ K. Shear thickening effects are also observed for PEO-UPY[18] and are commonly observed in complex fluids including dense suspensions, wormlike micelles, and associating polymer solutions.[60–62] In fact, shear thickening is not yet well understood in literature,[60–64] and thus several theoretical models have been proposed to describe the shear thickening behavior.[64–66] Marrucci et al.[64] explored the possibility of shear thickening as arising due to a non-Gaussian chain stretching effect. On the basis of the Tanaka and Edward transient network model, it is argued that under flow conditions polymer chains may elongate considerably, well into the non-Gaussian regime, as a result of chain stretching. In an extension, the free path model by Marrucci et al. further assumed that when the chain end dissociates from a network junction, it can only partially relax its extended conformation since it is soon recaptured by the network again. As a consequence, the maximum in the viscosity occurs at a critical shear rate when the ratio of the detachment frequency to the shear rate (which decreases monotonically with increasing shear rate) has not dropped to its asymptotic lower bound, and yet the polymer chains are already stretched close to their maximum extension. In the free path model, the critical shear

rate (shear rate at the maximum viscosity) is then estimated assuming that the elastically active chains reach full extension at the onset of shear thickening. In the case of PPO-upy, shear thickening is only observed at the two lowest temperatures, 283 K and 293 K, on contrary to PEO-UPY, where this effect is observed at the full measured temperature range.[18] Above T = 293 K , shear thinning is detected for PPO-UPY, where the viscosity decreases under shear strain.

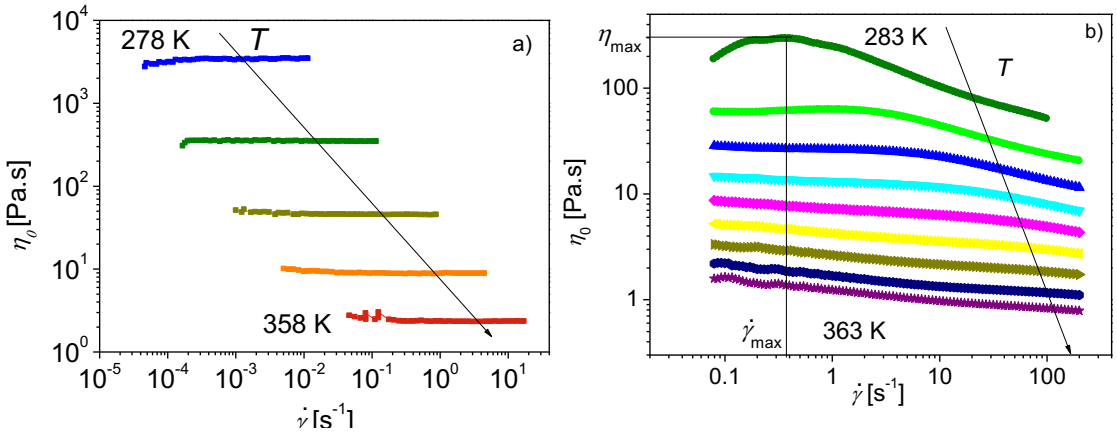

Figure 4. Zero-shear viscosity η_0 vs shear rates $\dot{\gamma}$ for a) PPO-THY/DAT (blue- 278 K, dark green- 298 K, light green- 318 K, orange- 338 K, dark red- 258 K) and b) PPO-UPY (dark green- 283 K, green- 293 K, blue- 303 K, cyan- 313 K, magenta- 323 K, yellow- 333 K, light green- 343 K, dark blue- 353 K, purple- 363 K). The black lines show the shear rate at the maximum viscosity for T = 283 K. The arrows indicate the direction of increasing temperature.

Figure 5a presents the time-temperature superposition (TTS) master curves of the shear modulus for PPO polymer and PPO-THY/DAT constructed by horizontal shifting of the shear modulus loss spectra, i.e., the storage (G') and loss (G'') moduli at different angular frequencies, until a best match with the spectra of the respective reference temperature, T_{ref} = 278 K, is

achieved. Although the underlying assumption of TTS may not be accurate for PPO-THY/DAT, the master curves can still provide a general picture of the mechanical properties.[12,17,56]

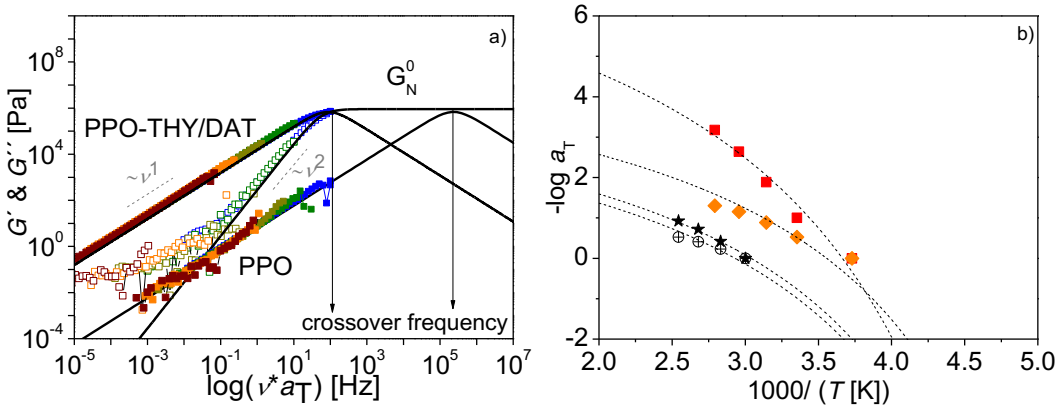

Figure 5. (a) Shear modulus master curves (G' open symbols, G'' closed symbols) as constructed from linear rheology oscillatoric measurements vs frequency ν at different temperatures (blue- 278 K, dark green- 398 K, light green- 318 K, orange- 338 K, dark red- 358 K) by TTS for PPO-THY/DAT and PPO backbone polymer as indicated for $T_{ref} = 278$ K. The black lines represent the fit to the data using equations (5) and (6). The dashed grey lines indicate characteristic slopes of the shear modulus in the terminal regime;b) the respective shift factors used to construct plot a). The dashed lines represent the temperature dependence of the dielectric α-relaxation time for PPO (orange diamonds), PPO-THY/DAT (red squares), PEO (black crossed circles) and PEO-THY/DAT (stars).

It is evident that for PPO-THY/DAT the slope of $G'' \approx 1$ and the slope $G' \approx 2$, and the viscous behavior dominates in both systems as seen from **Figure 5a**. The typical behavior of a Newtonian fluid is observed as for PPO backbone polymer. In this context, and taking into account the structural data, it is assumed that the associated chains can be described by the Rouse theory, as previously demonstrated under similar conditions for PEO-THY/DAT.[54] The ratio of the zero-

shear viscosities of PPO-THY/DAT and PPO polymer decreases from ~490 at T = 278 K to ~22 at T = 358 K, indicating a systematic de-association with increasing temperature, because otherwise these values would be constant. We assume that these values reflect the mass-averaged number of associated building blocks $\langle N_{\mathrm{assc}} \rangle_{\mathrm{w}}$, which clearly, as a consequence of the hydrogen bond interactions weakening, decreases with temperature. Moreover, in the Rouse regime, using the zero-shear viscosity, both the segmental relaxation time τ_{s}, as well as the expected Rouse time τ_{R}, can be extracted for PPO polymer by the following equations:[57,58,67,68]

$$\tau_{\mathrm{s}} = \frac{12 M_{\mathrm{n}} \eta_0}{\mathrm{N_A} N^2 \rho \pi^2 \mathrm{k_B} T} \tag{3}$$

$$\tau_{\mathrm{R}} = N^2 \tau_{\mathrm{s}} \tag{4}$$

where ρ is the density of the polymer melt, $\mathrm{N_A}$ the Avogadro number, $\mathrm{k_B}$ the Boltzmann constant and M_{n} and N are given above (these results for τ_{s} and τ_{R} are shown in **Figure 8a** below). In order to extract the terminal relaxation time, τ_{t} and compare it with the calculated Rouse time, a function composed of a generic peak function[12,17,56] to account for contributions of the chain dynamics is adjusted to the master curve data for PPO backbone (see **Figure 5a**):

$$G' = \mathrm{G_e} \frac{\omega^2 \tau_{\mathrm{t}}^2}{\omega^2 \tau_{\mathrm{t}}^2 + 1} \tag{5}$$

$$G'' = \mathrm{G_e} \frac{\omega \tau_{\mathrm{t}}}{\omega^2 \tau_{\mathrm{t}}^2 + 1} \tag{6}$$

where ω (= $2\pi\nu$) is the angular frequency, $\mathrm{G_e}$ represent the plateau moduli in the terminal regime and $\tau_{\mathrm{t}} = 1/\omega_{\mathrm{t}}$ is the characteristic relaxation time of the terminal relaxation. In order to do so, the common plateau modulus for PPO as in literature[69] is kept constant and the only free parameter is τ_{t}. The same fit procedure is done to the master curve data of PPO-THY/DAT using also equations (5) and (6). Clearly a visible crossover between G' and G'', corresponding to the terminal relaxation

time, τ_t and the typical features for the shear modulus spectrum of an unentangled polymer as mentioned above is observed. Particularly, at high frequencies the value of the plateau modulus is the same as for PPO backbone.[69] It is to note that this very rough approximation is not valid for rigorous analysis of the relaxation spectra. Failure of TTS in our case is reflected in the slight difference in the temperature dependency of the shift parameter a_T and the dielectric α-relaxation as it is shown in **Figure 5b**. However, this approximation is sufficient to estimate the characteristic relaxation times of the terminal modes (the values are represented in **Figure 8a** and **Figure 9** below). The obtained relaxation times refer to the reference temperature, $T_{ref} = 278$ K.

The relaxation time τ_d of the PPO-UPY network, is determined using the shear rate at the maximum viscosity, $\dot{\gamma}_{max}$, taken from the analysis of the steady-shear viscosity data in **Figure 4b** by: $\tau_d \approx 1/\dot{\gamma}_{max}$ (the obtained values are shown in **Figure 8c** and **Figure 10** below) at $T = 283$ K and $T = 293$ K . The UPY groups that aggregate as spherical clusters are the chain junctions and thus act as the network crosslinks. According to this picture, and taking into account the free path model described above,[64] τ_d is correlated with the detachment relaxation time of the PPO polymer chains from the network junctions, i.e., from the UPY clusters, assuming that the elastically active chains detach from the clusters at the onset of shear thickening. Additionally, from the oscillatory shear measurements (figure S7 in section IV of the S.I.), it is shown that the storage modulus G' dominates over the loss modulus G'' almost over all the studied frequency range. The slope of $G'' \approx \omega^{0.6}$, is lower than 1 ($G'' \approx \omega$), found for Newtonian systems or polymer melts at flow and typical of network-like systems. The elastic behavior dominates, as G' is relatively constant indicating that the plateau modulus $\sim 1.6 \times 10^4$ Pa at $T = 293$ K is lower than the plateau modulus $G_N^0 \sim 7.0 \times 10^5$ Pa at $T = 298$ K for PPO backbone polymer.[70] According to

simple rubber elasticity theory, the plateau modulus (G_N^0) for a supramolecular network is given by [63,71]:

$$G_N^0 = \nu_e k_B T = \frac{f_e N_A k_B T \rho}{M_{n,PPO-upy}} \quad (7)$$

where ν_e is the number density of elastically active strands, k_B is the Boltzmann constant, T is the absolute temperature, ρ is the density of the supramolecular polymer melt (1.0 g·cm^{-3}), N_A is Avogadro constant, $M_{n,PPO-UPY}$ is the supramolecular polymer molar mass (**Table 1**) and f_e is the fraction of bridging or elastically effective molecules. Considering a perfect network where all PPO chains adopt a bridging conformation between the UPY clusters and thus all would be elastically effective, f_e = 1 and $\nu_e \approx 392$ mol·m^{-3} at $T = 298$ K. In this case, the estimated plateau module $G_N^0 \sim 9.7 \times 10^5$ Pa for PPO polymer is retrieved.[37] While simple rubber elasticity theory overestimates G_N^0 of supramolecular PPO-UPY, the overestimation is not surprising. In fact, a lower value and an overestimation of the plateau modulus is also found for PEO-UPY and for systems that also form cluster-like structures due to H-bonding interactions.[18,39,63,72] Even though H-bonding can create crosslinks that built the network, it also introduces defects formed due to loops existence, lowering G_N^0. Indeed, the possibility of PPO chains to form loops within the same cluster instead of bridges to different clusters has to be considered and can explain the lower f_e (see further in the text). Besides that, probable contributions from PPO-UPY functionalized at only one chain end, which stem from incomplete reaction steps during the functionalization of the polymeric product with subsequent different propensities (see **Table 1**), inevitably contribute to a lower fraction of effective elastically molecules between the UPY crosslinks. In this context, the lower value of G_N^0 found for PPO-UPY can be rationalized to a bridging fraction $f_e \approx 0.02$ at $T = 293$ K. Definitely the observation of a plateau modulus clearly shows that the liquid-like

viscoelastic properties of PPO at the studied molar mass have changed into a network-like due to the presence of the UPY end groups, in accordance with what is observed above by small angle scattering.

The molar density of elastically active strands calculated using equation (7) at $T = 333$ K is $\nu_e = 1.4$ mol·m^{-3}, which is very comparable with the value obtained by small angle scattering ($\nu_e = 1.0$ mol·m^{-3}- 1.3 mol·m^{-3}). Undeniably, these values are in very good agreement to the values calculated using the rheology data for the same temperature.

3.2.3. *Dielectric Relaxation Spectroscopy*

The derivative spectra of the real part of the dielectric permittivity of PPO, PPO-THY/DAT and PPO-UPY are presented in **Figure 6**: [35]

$$\varepsilon''_{\mathrm{deriv}}(\omega) = \frac{-\pi}{2}\frac{\partial \varepsilon'(\omega)}{\partial \ln \omega} \qquad (8)$$

This representation can help to unravel relaxation processes, which are obscured by Ohmic conductivity or adjacent processes in the loss spectra. Hence this representation is used to analyze the dielectric data because it circumvents conductivity contributions and allows to unravel dipolar mechanisms that are masked in the typical loss spectra $\boldsymbol{\varepsilon}''$. While this representation suppresses totally the contribution of dc conductivity to the dielectric loss $\boldsymbol{\varepsilon}''$, this is not the case for electrode polarization (EP)and Maxwell-Wagner-Sillars (MWS) mechanism. Nevertheless, it is still a very useful approach for handling such phenomena by enabling to unravel genuine relaxation processes, for example, by observing if the curves of $\varepsilon''_{\mathrm{deriv}}(\omega)$ at the high frequency side fall off with $\varepsilon''_{\mathrm{deriv}} \propto \omega^{-2}$, which is typical for EP effects.[35]

The derivative spectra of PPO in **Figure 6** reveal three relaxation processes:[56] (i) the dielectric α-relaxation at high frequency that represents the segmental relaxation, (ii) the normal mode (NM) at lower frequency that represents the end-to-end relaxation (chain modes) characteristic for type

A polymers[73] and iii) at temperatures higher or frequencies lower than the normal mode process (**Figure 6a**), a less intense process is observed, which persists active in almost the whole studied temperature range, even for temperatures higher than α- and NM processes. Concerning the derivative spectra of the supramolecular polymers, we observe only two processes for PPO-THY/DAT, while the spectra of PPO-UPY exhibit also three relaxation peaks similar to PPO polymer (**Figure 6c**). The assignment of the observed relaxation processes will be discussed further in more detail.

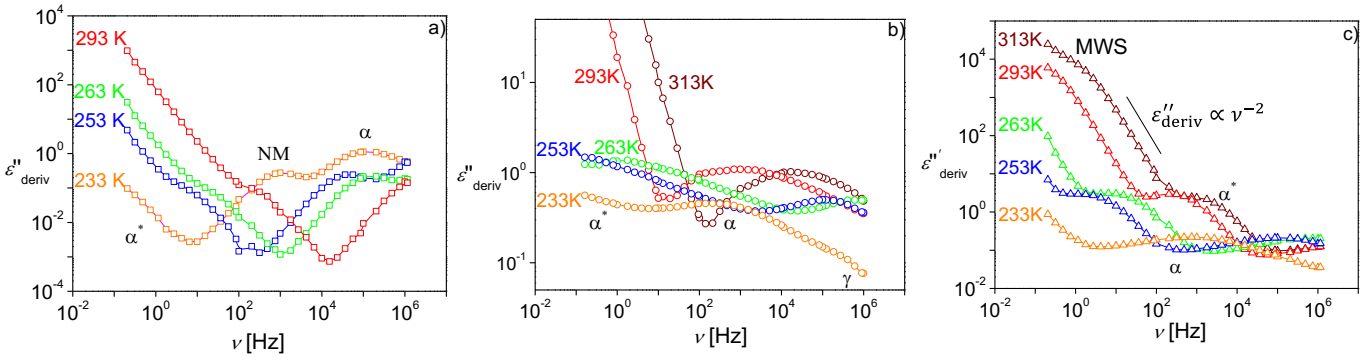

Figure 6. Derivative of the dielectric permittivity spectra for a) PPO, b) PPO-THY/DAT and c) PPO-UPY shown for different temperatures as indicated.

The dielectric spectra are normally analysed by fitting a sum of the Havriliak–Negami (HN) function:[35,73]

$$\varepsilon^*(\omega) = \varepsilon_\infty + \sum_{\mathrm{k}} \frac{\Delta\varepsilon_{\mathrm{k}}}{[1 + (\mathrm{i}\omega\tau_{\mathrm{HN}})^{\alpha_{\mathrm{HN_k}}}]^{\beta_{\mathrm{HN_k}}}} \tag{9}$$

The derivative-based loss spectra $\varepsilon''_{\mathrm{deriv}}(\omega)$ from equation (8) are analyzed by the analytical derivative of the HN function[35]

$$\frac{\partial\varepsilon'(\omega)}{\partial \ln \omega} = -\frac{\alpha_{\mathrm{HN}}\alpha_{\mathrm{HN}}\Delta\varepsilon(\omega\tau_{\mathrm{HN}})^{\alpha_{HN}} \cos[(\pi\alpha_{\mathrm{HN}}/2) - \theta_{\mathrm{HN}}(1 + \beta_{\mathrm{HN}})]}{[1 + 2(\omega\tau_{\mathrm{HN}})^{\alpha_{HN}} \cos(\pi\alpha_{\mathrm{HN}}/2) + (\omega\tau_{\mathrm{HN}})^{2\alpha_{\mathrm{HN}}}]^{(1+\beta_{\mathrm{HN}}/2)}} \tag{10}$$

With $\theta_{\mathrm{HN}} = \arctan[\sin(\pi\alpha_{\mathrm{HN}}/2)/((\omega\tau_{HN})^{-\alpha_{\mathrm{HN}}} + \cos(\pi\alpha_{\mathrm{HN}}/2))]$ and k sums over the different relaxation processes, ω is the angular frequency ($\omega = 2\pi\nu$), τ_{HN} is a characteristic relaxation time that is related to the frequency of maximal loss ν_{max}, $\Delta\varepsilon$ is the dielectric relaxation strength of the process under investigation and ε_∞ is the high frequency limit of the real part $\varepsilon'(\omega)$; α_{HN} and β_{HN} are fractional shape parameters ($0 < \alpha_{\mathrm{HN}} \leq 1$ and $0 < \alpha_{\mathrm{HN}} \cdot \beta_{\mathrm{HN}} \leq 1$) describing the symmetric and asymmetric broadening of the dielectric spectrum.

From the estimated values of τ_{HN}, α_{HN}, and β_{HN}, a model- independent relaxation time τ_{max} $\left(\nu = \nu_{\mathrm{max}} = 1/(2\pi\tau_{\mathrm{max}})\right)$ is calculated according to ref. [73]:

$$\tau_{\mathrm{max}} = \tau_{\mathrm{HN}} \times \left[\sin\left(\frac{\alpha_{\mathrm{HN}}\pi}{2 + 2\beta_{\mathrm{HN}}}\right)\right]^{-1/\alpha_{\mathrm{HN}}} \left[\sin\left(\frac{\alpha_{\mathrm{HN}}\beta_{\mathrm{HN}}\pi}{2 + 2\beta_{\mathrm{HN}}}\right)\right]^{1/\alpha_{\mathrm{HN}}} \quad (11)$$

The characteristic relaxation frequency resulting from the fits to the data of both $\varepsilon''_{\mathrm{deriv}}$ and loss spectra $\boldsymbol{\varepsilon}''$ representations for all the visible dielectric processes of PPO are equivalent, confirming the accuracy of the fits and the extracted parameters can thus be considered as comparable (section V of the S.I.). **Figure 7** gives three representative examples of the used fitting procedure for all studied systems at the same temperature for a better comparison. The so-obtained parameters, spectral shape and dielectric strength, as well as the relaxation time for each process are discussed in the following in detail.

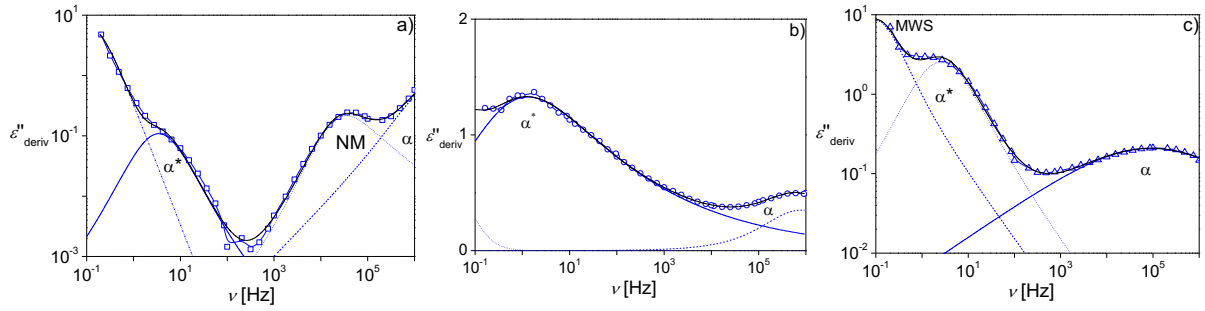

Figure 7. Derivative of the dielectric permittivity spectra of (a) PPO, (b) PPO-THY/DAT and (c) PPO-UPY, at *T* = 253 K. The black solid lines are the overall fit to combinations of HN

functions. The blue solid, dashed and dash-dotted lines indicate the individual contributions of different relaxation processes.

Spectral Shape

It is well established that the derivative analysis yielding $\varepsilon''_{\mathrm{deriv}}(\omega)$ alters the spectral shapes by a slight peak sharpening in comparison to the dielectric loss spectra peaks.[35] However, the fit with the respective equations to the different representations revealed a not so different values of the shape parameters (Table S4, S5 and S8 in section V of the S.I.). In this context, hereby a short analysis.

The shape of the segmental relaxation for all studied systems has a relatively weak temperature dependence, $\alpha_{HN,\alpha} \approx 0.77$; , $\alpha_{HN,\alpha} \cdot \beta_{HN,\alpha} \approx 0.47$, $\alpha_{HN,\alpha} \approx 0.50$; $\alpha_{HN,\alpha} \cdot \beta_{HN,\alpha} \approx 0.44$, $\alpha_{HN,\alpha} \approx 0.45$; $\alpha_{HN,\alpha} \cdot \beta_{HN,\alpha} \approx$ 0.45 for PPO, PPO-THY/DAT and PPO-UPY, respectively. However, for the supramolecular polymers an increase in broadness is observed that seems to increase with increasing Flory-Huggins parameter, from THY/DAT to UPY. The broadening of the segmental relaxation can be interpreted as an increase in heterogeneity, related with changes in intra- and inter-molecular interactions in the cooperative conformational movements that originate this relaxation process. The α^*-process that shows up in the low frequency flank is characterized by a Debye-like behavior for PPO-UPY ($\alpha_{HN,\alpha^*} = 1$; $\beta_{HN,\alpha^*} = 1$) and PPO ($\alpha_{HN,\alpha^*} \approx 0.97$; $\beta_{HN,\alpha^*} = 1$), while the peak of the α^*-process for PPO-THY/DAT is broad ($\alpha_{HN,\alpha^*} \sim$ 0.48 and asymmetric ($\alpha_{HN,\alpha^*} \cdot \beta_{HN,\alpha^*} = 0.22$). In fact, a Debye-type process is observed in a variety of associating liquids, related to hydrogen bonding dynamics. In the case of PPO-THY/DAT, increase in broadness can also indicate heterogeneity as here there are two different H-bonding components playing a role on the association dynamics. Concerning the normal mode relaxation peak for PPO

is relatively narrow, and the asymmetry decreases with temperature, ($\alpha_{HN,NM} \approx 0.94 \pm 0.04$; $\beta_{HN,NM}$ = 1,0 - 0.6, as expected.[26,27] Finally, for PPO-upy the peak observed at frequencies lower than the α^*-process has a purely Debye character.

Dielectric Strength

The starting point for the analysis of Δε is the extension of the Debye theory by Onsager, Fröhlich, and Kirkwood (see [73,74] and references therein).

$$\Delta\varepsilon = \frac{\mu_0^2}{3\varepsilon_0} gF \frac{1}{\mathrm{k_B}T} \frac{N}{V} \tag{12}$$

ε_0 is the vacuum permittivity, μ_0 the dipole moment of the moving unit in vacuum, $F \approx 1$ is the Onsager factor calculated in the frame of the reaction field, T the temperature, $\mathrm{k_B}$ the Boltzmann constant, N/V the number density of dipoles, $\mathrm{N_A}$ is Avogadro's number and g is the Kirkwood/Fröhlich correlation factor to take into account short-range intermolecular interactions that lead to specific static dipole–dipole orientations. In the particular case of a monodisperse type A polymer, the dielectric strength of the α-relaxation is escribed as[73,75–77]

$$\Delta\varepsilon_\alpha = \frac{4\pi\tilde{\mu}^2}{3} gF \frac{1}{\mathrm{k_B}T} \frac{X\mathrm{N_A}\rho}{M_n} \tag{13}$$

here μ˜ is the dipole moment of the repeat unit, X is the degree of polymerization ($X\mathrm{N_A}\varrho/M_\mathrm{n}$ is the number density of repeat units), M_n is the polymer molar mass and ϱ is the density. The $\Delta\varepsilon_\alpha$ values decrease with increasing temperature for all studied polymers and the absolute values decrease from PEO to PEO-THY/DAT and PEO-UPY, α ~3.69 (213 K) → 3.08 (243 K), α ~2.11 (233 K) → 1.19 (263 K), α ~ → 1.35 (213 K) → 0.76 (253 K), respectively. Since the dipole moment of the repeat unit is the same, the observed decrease of $\Delta\varepsilon_\alpha$ with T seems to be due to enhanced correlations among the dipoles, while the decrease of the absolute $\Delta\varepsilon_\alpha$ values with

functionalization and the Flory-Huggins parameter appears to be due the increase of the polymer molar mass as a consequence of association and network formation.

$$\Delta\varepsilon_{\mathrm{NM}} = \frac{4\pi\tilde{\mu}_{\mathrm{p}}^2}{3} gF \frac{1}{\mathrm{k_B}T} \frac{\mathrm{N_A}\rho}{M_{\mathrm{n}}} R_{\mathrm{e}} \tag{14}$$

Concerning the dielectric strength of the normal mode, $\Delta\varepsilon_{\mathrm{NM}}$,[73,77,78] described in (14) where $\tilde{\mu}_{\mathrm{p}}$ is the dipolar moment per unit length of the repeat unit parallel to the backbone and R_{e} is the mean-square end-to-end distance of the chain. Like for the segmental relaxation, the $\Delta\varepsilon_{\mathrm{NM}}$ values for PPO increase in intensity with decreasing temperature, this can be also attributed to the increase correlations among the dipole but it can also be due primarily to an increase of R_{e} with decrease T, as a result of H-bonding association.

Finally, regarding α^*-process, the $\Delta\varepsilon$ values, which is proportional to the amount of participating dipoles, are fairly temperature independent for PPO ($\Delta\varepsilon = 0.05 \pm 0.01$) and PPO-UPY ($\Delta\varepsilon = 5.89 \pm 0.79$), but decreases with T for PPO-THY/DAT ($\Delta\varepsilon \sim 9.31$ (263 K) → 5.77 (313 K), which seems to point out that the number of contributing dipoles to this relaxation increases from PPO, to PPO-UPY and PPO-THY/DAT, inverse to the Flory-Huggins interaction parameters. This appears to agree to the structural picture describe above.

Relaxation map

Figure 8 shows the temperature dependence of the characteristic relaxation frequency ν $\left(\nu = \nu_{\max} = 1/(2\pi\tau_{\max})\right)$ for all relaxation processes analyzed. The temperature dependence of the mean relaxation times for the α-relaxation (the faster process in the studied temperatures), is curved when plotted versus 1000/T. Close to T_{g}, this dependency is often described by the empirical Vogel-Fulcher-Tammann-Hesse (VFTH) equation:

$$\tau_{\max}(T) = \tau_0 exp\left(\frac{B}{T - T_0}\right) \tag{15}$$

where τ_0 and B are fitting parameters and T_0 is the so-called Vogel temperature found to be 50 to 70 K below T_g. From these parameters, also the fragility index m can be calculated:

$$m = \frac{\mathrm{B}T_g^{\mathrm{diel}}}{\ln 10 \left(T_g^{\mathrm{diel}} - T_0\right)^2} \tag{16}$$

which indicates the steepness of the temperature dependence of the relaxation time at T_g and is considered to reflect the frustration in molecular packing (**Table 3**).[12,17,56]

The dielectric glass transition temperature values determined by extrapolating the Vogel–Fulcher–Tammann-Hess (VFTH) equation (equation (15) fit to the dielectric data T_g^{diel} (τ = 100 s) are 199±9 K, 213±15 K and 209±12 K, respectively, for PPO, PPO-THY/DAT and PPO-UPY, being in close agreement with the calorimetric $T_{g,DSC}$ (see **Table 2** above). The dielectric glass transition temperature of PPO, 204.8 K, is also in perfect agreement with 205.2 K of ref. [46].

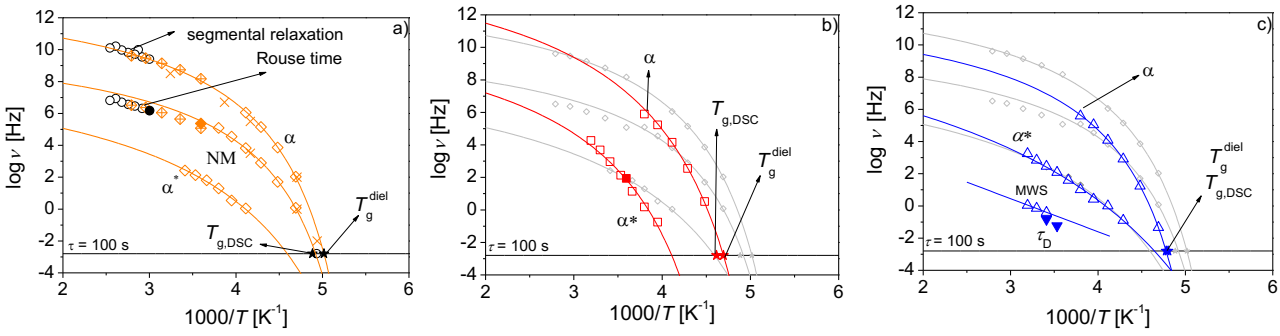

Figure 8. Temperature dependence of the characteristic relaxation frequencies for a) PPO polymer (orange diamonds), including the segmental relaxation time and Rouse time calculated with PPO zero shear viscosities using the Rouse equation (crossed diamonds) as well as the terminal time for PPO (full symbols). The characteristic frequency times of α-relaxation and normal mode from similar molar mass PPO polymer taken from literature[26,79]

is also presented (orange times symbols). The Rouse time and segmental relaxation time for PEO is taken from ref. [18] (black open circles) and the calculated terminal time for PEO (full black circle) are also included (Figure S8 in section IV in the S.I.), b) PPO-THY/DAT (red squares) in comparison with PPO polymer (gray). It includes also the terminal time for PPO-THY/DAT (full symbols), c) PPO-UPY (blue triangles) in comparison with PPO polymer (gray symbols). The shear rate frequency at the maximum viscosity, $\boldsymbol{\nu_D = 1/(2\pi\tau_D)}$ for PPO-UPY (full faced down triangles) is also included.

This helps to identify the segmental relaxation among several other processes observed in the DRS spectra. The assignment of the α-relaxation to the segmental relaxation is corroborated by the fact that T_g^{diel} values obtained by equation (15) to a timescale of about 100 s coincides with the glass transition temperature $T_{g,DSC}$ obtained from calorimetric measurements (see **Figure 9**), to note that the Vogel temperature ($T_{0,\alpha}$) for all the polymers is very alike, i.e., the viscosity and the structural relaxation time extrapolate to infinity at the similar temperature. The α-relaxation for all three polymers seems to have a similar origin, which is expected since this process is related to the local mobility covering only few repeating monomer units.

Table 3. Fitting parameters for the temperature dependence of the different relaxation times found for PPO polymer, PPO-THY/DAT and PPO-UPY.

Relaxation	System	log (τ_0) [s]	B [K]	T_0 [K]	*m*
α	PPO	-15.3±0.4	340±33	171.5±2.5	88±32
	PPO-THY/DAT	-18.2±1.6	518±145	172.2±8.4	66±6
	PPO-UPY	-14.1±0.5	331±32	176.3±2.0	64±18
NM	PPO	-12.0±1.8	292±85	170.6±6.8	61±19

α^*	PPO	-11.4±6.6	570±238	155.4±24.9	32±13
	PPO-THY/DAT	-14.1±1.3	423±118	176.3±9.6	23±5
	PPO-UPY	-16.2±7.0	1283±443	129.6±27.8	31±6

Moreover, in supramolecular polymers with H-bonding end groups, typically an additional relaxation process can be found that is not the normal mode process.[12,17,56,80,81] Mobility associated with the normal mode directly reflects the motion of the end-to-end chain and only affects polymers with a dipole parallel to the chain contour, "type-A" polymers, like PPO. In the case of the associating chains functionalized at both ends, it should not be observed. The reason is that for the normal mode to appear in the dielectric spectra, each repeating unit must have a component of its dipole moment that is parallel to the main chain, and additionally this component must be directed towards the same end of the chain in all repeating units. Only if the chemical structure of the polymer satisfies these conditions, the dipole moments can add up along the contour of the chain and give rise to an end-to-end dipole. In associating polymers, however, there is no mechanism that directs the end-to-end dipoles of the contributing chains towards the same end of the chains. Consequently, these end-to-end dipoles have random orientations towards both ends of the associating chains. Thus, on average the dipole moments along these chains cancel out.[12,56,80] The relaxation process, which is found a few decades slower than the α-relaxation and exhibits a similar temperature dependence as it can be clearly observed in **Figure 8b** and **c** for PPO-THY/DAT and PPO UPY, is ascribed to the dissociation process of hydrogen bonds; this leads to a change of dipole moment due to the change in the distance between the partial charges of the hydrogen bond donor and acceptor atoms.[12,17,56,81] Hence it is called α^*-relaxation. For PPO, besides the segmental and chain relaxation processes, i.e., α and normal mode relaxations, in order of decreasing frequencies, the α^*-process is revealed at even lower frequencies, but only in the

derivative representation. This is because this representation eliminates the conductivity effects that tend to mask dipolar contributions, specially at high temperatures. This slower process, named α*-process is described by a Debye-like relaxation function, i.e., the shape parameters used in the analytical derivative of the HN function[35] to fit the data are close to 1, and the temperature dependence of relaxation time follows the VFTH behavior. These are all features of the so-called Debye process traditionally found in monohydroxy alcohols, related to the hydrogen-bond dynamics.[82] Added to this, recently, it has been established that this slow process is related to the formation of hydrogen-bonded polymer-like structures in supramolecular polymers, such as hydroxy terminated PDMS[17,56] and acid terminated PPO[12,56]. Particularly in this work, where we deal with dihydroxy terminated PPO, hydrogen bonds within the OH groups at the chain ends are possible and thus the assignment of this process as α*-relaxation.

Figure 8 shows that the temperature dependence of the relaxation times for the α*-relaxation for PPO, PPO-THY/DAT and PPO-UPY is also curved when plotted versus 1000/*T*, thus a fit to the data using the VFTH equation (equation (15) is also appropriate. Interestingly, the Vogel temperatures of both the α*-relaxation and α-relaxation for PPO-THY/DAT, are very comparable, therefore for PPO-THY/DAT some correlation seems to exist between both relaxation processes. Assuming that the α*-relaxation is connected with the dissociation process of hydrogen bonds, the similarity of its temperature dependence with that of the main α -relaxation is an indication that the dynamics of the former is governed by the dynamics of the α –relaxation. In the case of both PPO-UPY and PPO, $T_{0,\alpha^*,}$ is different from $T_{0,\alpha}$ of the respective main relaxation, which leads to the conclusion that in this case the dynamics is not governed by the α –relaxation as for PPO-THY/DAT. Indeed the dynamics and temperature dependence of the α^*-relaxation coincides in

both PPO-UPY and PPO as supported by the dielectric spectra present in **Figure 8c**. Thus for both systems the assignment of this process is the same.

Moreover, concerning the assignment of the α^*-relaxation for PPO-THY/DAT, the construction of the master curves from the shear modulus spectra using TTS (**Figure 5**) has proven to be a valuable tool.[17,56] Of particular interest are the characteristic times of the rheological processes (such as the terminal relaxation) as well as the respective plateau modulus. In **Figure 8b** it is shown the good agreement between the relaxation time of these slow dielectric process and of the terminal relaxation time at the reference temperature for PPO-THY/DAT (see **Figure 5**). In fact, according to Cates model,[83] when the lifetime of the association is much shorter than the characteristic time for the chain dynamics, the plateau modulus of the associated polymer should be similar to that of the conventional covalently-bonded polymer of the same backbone and the terminal relaxation should be dominated by a single Maxwell relaxation. This is visible in **Figure 5b** and put in evidence in **Figure 8b**. **Scheme 1a** is representing the molecular view as predicted by the model.

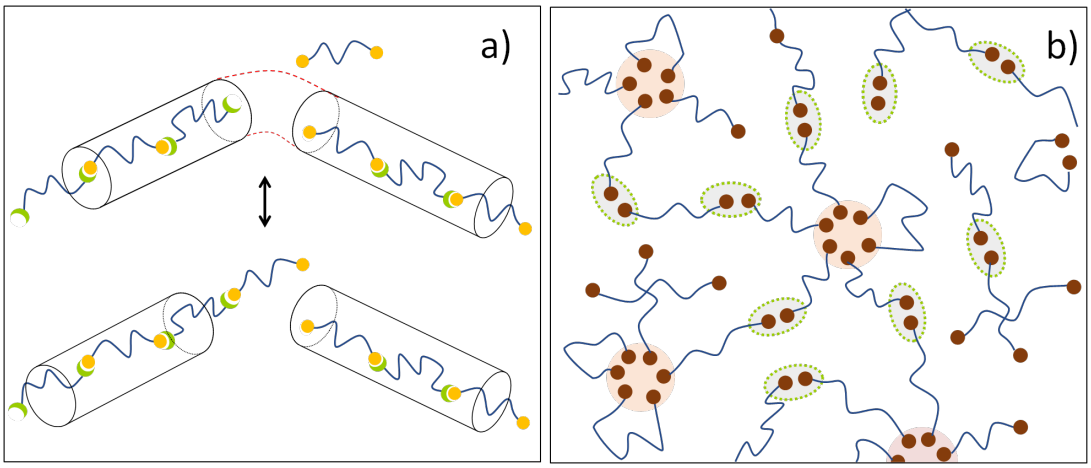

Scheme 1- Schematic illustration of: a) the relaxation mechanisms as presented in Cates model: the polymer segment relaxes over the break which occurs within a certain distance along the chemical sequence; the break must be close enough that the newly released end can move through the polymer segment before it recombines with a neighboring chain. b) the

association structure of PPO-UPY with small transient bonds, presumably dimers, and larger effectively permanent bonds, denoted here as clusters.

Besides the α^* −relaxation, the dielectric spectra of PPO-UPY reveal a third peak at elevated temperatures (**Figure 6c** and **Figure 7c**). This process is analysed with equation (10) to extract its characteristic frequencies, which exhibits in the studied temperature range a linear dependence when plotted versus $1000/T$ in **Figure 8**c. Accordingly, the Arrhenius equation is used to fit the data:[34,73]

$$\tau = \tau_0 \mathrm{e}^{E_\mathrm{a}/\mathrm{R}T} \tag{17}$$

where τ_0 is the relaxation time at infinite temperature that for the case of a molecule is related to the time needed to move into some free space, [34,73] R is the ideal gas constant and E_a is the activation energy. The values of the activation energy are present in **Table 4** and will be discussed in the next section.

Interestingly, this slowest process characteristic times are very close to the relaxation times of the PPO-UPY network τ_d, determined using the shear rate at the maximum viscosity (**Figure 4**), which basically indicates the detachment relaxation time of the PPO chains from the network junctions, i.e., from the UPY clusters,[18,64,71] as shown in **Figure 8c**. However, looking to **Figure 6c** and **Figure 7c**, the dielectric strength, $\Delta\varepsilon$ is in the order of 10^3 (see table S8 in section V of the S.I.), higher than the values found for typical dipolar relaxations but rather typical of electrode polarization or Maxwell-Wagner-Sillars mechanism.[35] Moreover, in **Figure 6c**, the lowest frequency peak shows a power law as $\varepsilon''_{\mathrm{deriv}} \propto \omega^{-2}$, which can be typical for EP effects.[35]

This mechanism is explained by the accumulation of charge carriers in the electric field at the interface of two phases with large differences in conductivity and permittivity. The hopping

relaxation time of these charge carriers at the interface can give rise to an additional relaxation process. Therefore, this is normally found in inhomogeneous media and it suggests phase separation in the material itself. As it is known, the structure of PPO-UPY is network –like with UPY clusters acting as crosslinks, which can then work as possible polarisable boundaries. Consequently, the coincidence between i) this slowest process in the dielectric data of PPO-UPY and ii) with the detachment relaxation time of the PPO-UPY chains taken from rheology does not seem surprising.[80] In fact, the Arrhenius activation energy of this process is 39 kJ·mol^{-1} (**Table 4** below), which matches with reported values for the network detachment relaxation time for PEG-UPY[18] (45 kJ·mol^{-1}) and it is also comparable with the activation energy of the detachment relaxation time of the PPO-UPY (~55 kJ·mol^{-1} in **Table 4** below). Still, to draw decisive suppositions here is difficult given not only the complexity of the data and but also the rather limited data set.

Scheme 1b presents a possible illustration of the association structure of PPO-UPY with small transient bonds, presumably dimers, as the origin for the α^*-relaxation and larger effectively bonds, denoted here as clusters, responsible for the network-like behaviour shown in **Figure 4b** (and possibly creating an interface partially blocking charges between the PPO and UPY-rich domains and involving the dissociation dynamics of UPY groups within these clusters).

Finally, regarding the fragility index of the α-relaxation in both PPO-THY/DAT and PPO-UPY takes values on average of around 65 lower than the typical high value (around 90) for the unfunctionalized PPO chains.[26,27] According to the generalized entropy theory,[17,56,84–86] the fragility is considered to reflect the frustration in molecular packing.[17] Apparently, the chain end associations reduce the packing frustration of PPO segments. This is even more evident for the fragility values of the α^*-relaxation, which for all systems has much lower values of around 20-

30. Such low values are characteristic of H-bonding systems,[12] which is consistent with our assignment to a structural relaxation of a phase consisting of (hydrogen bond rich) chain ends.

3.3. Comparison

The understanding of the main chain polarity role is essential for a fundamental view on the underlying mechanisms triggering the different properties of supramolecular poly(alkyl ether) polymers. Therefore, a discussion of the key differences between the structure and dynamics of the respective PPO and PEO supramolecular polymers possessing at the ends the same H- bonding types is presented next.

3.3.1. *Structure*

SAS results have shown that both PPO-THY/DAT and PEO-THY/DAT associate into linear structures, proofed qualitatively by the Q^{-2} dependence at high Q and by the accurate description of the data by the RPA model,[18,29,30] while both backbone polymers carrying UPY at the ends presents a more compact phase segregated structure, consisting of a suspension of hard spheres with repulsive interaction, visible by the Q^{-4} dependence at intermediate Q range and quantitatively by the good fit with Percus- Yevick model to the SANS data. These observations are well evidenced in **Figure 2** and **Figure 3**, respectively.

However, though both PPO-THY/DAT and PEO-THY/DAT create a linear associating polymer, the number of associated building blocks $\langle N_{\mathrm{agg}} \rangle_{\mathrm{w}}$, is higher for PPO-THY/DAT at the same temperature, $\langle N_{\mathrm{agg}} \rangle_{\mathrm{w}} \geq 19$ at $T = 338$ K in comparison with $\langle N_{\mathrm{agg}} \rangle_{\mathrm{w}} \approx 15$ at $T = 333$ K[30] for PEO-THY/DAT. Indeed the higher hydrophobicity of the PPO-chains that are less polar than PEO-chains facilitates the association.

Concerning the UPY systems, the phase segregation in spherical clusters is less marked for the PPO-UPY case, just by considering the polydispersity parameter taken from the fit with the

Perkus-Yevick approach. It changes from around 11% in the PEO-UPY to ~40% for PPO-UPY.[18] In fact, the structure of PPO-UPY, as represented in **Scheme 1b**, seems to follow much closer the concept of a dual network than in the PEO case.[18] More, the rheology results revealed, on the one hand, the clear network-like behavior, but on the other hand a combination of shear-thinning and shear-thickening, instead of only shear-thickening as in the case of PEO-UPY in the full studied temperature range.[18] For PPO-UPY, shear thickening is observed but only at the two lowest studied temperatures as observed in **Figure 4b**. Both shear thickening and shear thinning effects are typically observed in systems that reveal phase separation, tough the latter is more typically observed on polymer melts and on systems where polymers play a bigger role.[70,80] In this context, for PPO-UPY samples, the structure seems to be mostly defined by the PPO characteristic relaxation times as also perceived in **Figure 8c** by the similar dielectric spectra in comparison with PPO. Remarkably, in the case of PPO-UPY, two very different types of bonds, i.e. small associates and clusters, are formed by the same species of end group establishing the dual network behavior: (i) some type of transient bond which releases stress by a transient network mechanism controlled by the characteristic times of association/dissociation between pairs of end groups involving most probably just two chain ends as in PPO and (ii) some much more stable type of bond or associate that forms the UPY clusters, which requires elevated temperatures to be dissociated. Naturally, surrounding these groups, many PPO chains as loops are observed (based also on the lower than expected plateau modulus from rheology) and the distance between the disordered UPY spheres is defined by the PPO end-to-end distance. This picture is based on the parameters from the Percus–Yevick approximation fit to the small scattering data for PPO-UPY that match very well with the structural characteristics of PPO polymer.

3.3.2. Dynamics

Figure 9a presents the temperature dependence of the segmental relaxation frequency for both PPO polymer and PPO-THY/DAT and the Rouse time for PPO polymer. The segmental relaxation time for both PEO polymer and PEO-THY/DAT and the Rouse time for PEO polymer are also presented in comparison.[18] Moreover, in **Figure 9b** the temperature dependence of the segmental relaxation frequency for PPO-UPY in comparison with PEO-UPY and with PPO and PEO polymer backbones, respectively is represented too.[18]

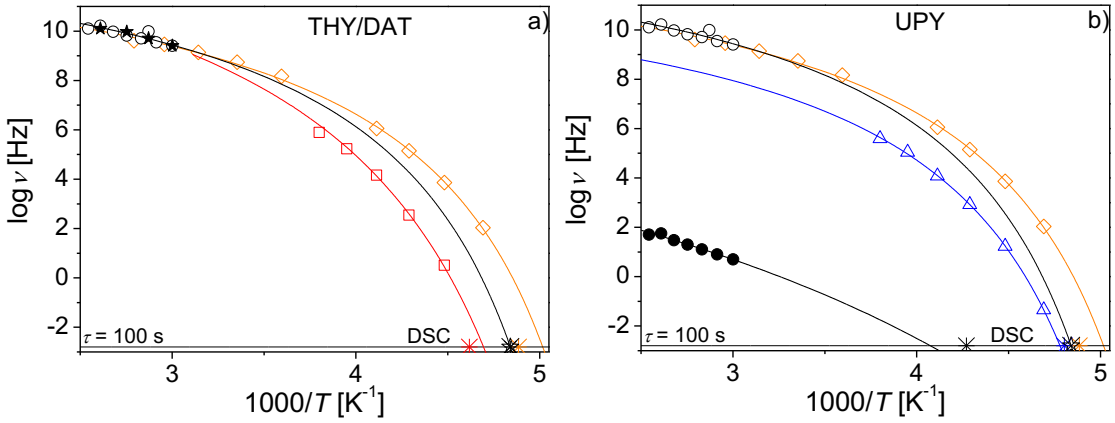

Figure 9. - Temperature dependence of the characteristic segmental relaxation frequencies for a) PPO (orange diamonds) and PPO-THY/DAT (red squares) in comparison with PEO (open black circles) and PEO-THY/DAT (black stars), b) PPO-UPY (blue triangles) and PEO-UPY (full black circles) network longest relaxation time, τ_c in comparison with PPO (orange diamonds) and PEO (open black circles) segmental relaxation times. The symbols at the horizontal line indication τ= 100 s are the corresponding calorimetric glass transition for the different systems at the same colors as the dielectric and rheological data. The lines are the fits to the data using the VFT equation. The colour of the lines is the same as the symbols. The respective fit parameters are present in Table 3.

It is observed that both the segmental relaxation time and the glass transition is influenced by the H- bonding groups. Indeed, the segmental relaxation time slows down due to association.

However, this influence differs with the poly(alkyl ether) chain polarity that the end groups are attached. For supramolecular PPO-UPY, the segmental relaxation is less influenced by the hydrogen-bonding association strength and the Flory-Huggins interaction parameter, than for PEO-UPY. The glass transition for PEO-UPY has the highest value either in comparison with PEO-THY/DAT, either in comparison with the supramolecular PPO polymers.

Figure 10 show the temperature dependence of the α*-relaxation frequency for both PPO-THY/DAT and PPO-UPY and for PPO backbone polymer too. The temperature dependence of MWS frequency for PPO-UPY is also represented. The temperature dependence of the literature values for the bond breaking frequencies ($\nu_{\mathrm{b}} = 1/(2\pi\tau_{\mathrm{b}})$), of a similar PEO-THY/DAT obtained by neutron spin-echo spectroscopy (NSE) is included,[54,68] as well as the PPO-UPY and PEO-UPY network detachment relaxation frequencies, $\nu_{\mathrm{d,PPO-UPY}}$ ($\nu_{\mathrm{d,PPO-UPY}} = 1/(2\pi\tau_{\mathrm{d,PPO-UPY}})$), and $\nu_{\mathrm{d,PEO-UPY}}$ ($\nu_{\mathrm{d,PPO-UPY}} = 1/(2\pi\tau_{\mathrm{d,PPO-UPY}})$), respectively. The values of τ_b represent the characteristic time scale of hydrogen bond breaking in the PEO supramolecular compounds.[54] Clearly, the temperature dependence of τ_b is on the one hand compatible with the terminal time estimated at T_{ref} = 333 K by the fit to the PEO-THY/DAT master curve with equation (6) and on the other hand with the values of the α*-relaxation of PPO-THY/DAT. The latter reflect the lifetime of the association/dissociation process of the hydrogen bonds established between THY/DAT groups attached to the PPO chain, i.e. a chemical relaxation that will generate a dielectric response by changing the combined dipole moments. Interestingly, it seems that the temperature dependence of the characteristic time scale of hydrogen bond association/dissociation is independent of the poly(alkyl ether) chain polarity that is attached, i.e., PPO and PEO, when the molecular mass of the backbone is lower than M_{e}. We assume that this is due to the fact that the lifetime of the association is shorter than the characteristic time for the chain dynamics, and the

plateau modulus of the "living" polymer is thus similar to that of the conventional covalently-bonded polymer of the same backbone.[83]

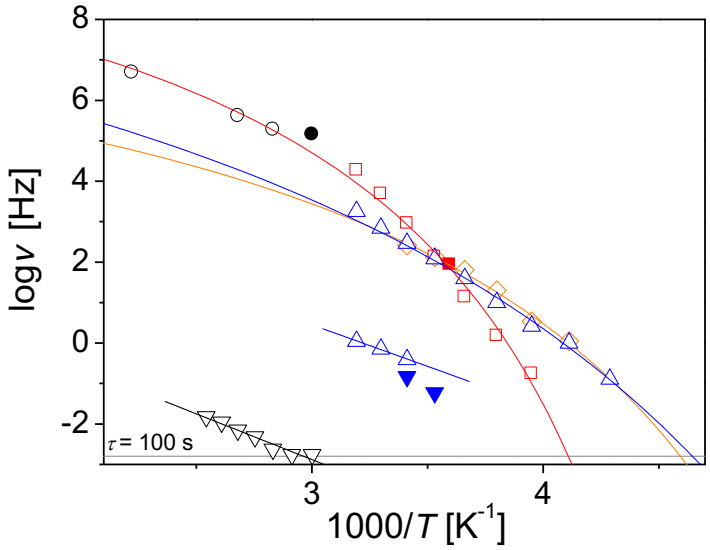

Figure 10. Temperature dependence of the characteristic relaxation frequencies of the hydrogen bonding dynamics for PPO (orange diamonds), PPO-THY/DAT (red squares), PPO-UPY (open blue triangles) in comparison with PEO-THY/DAT (open black circles) bonding frequencies studied by neutron spin eco spectroscopy (NSE)[54] and PEO-UPY network detachment relaxation frequency, $\nu_{d,PEO-upy} = 1/(2\pi\tau_{d,PEO-UPY})$, (open black face down triangles). The full black circle is the terminal frequency for PEO-THY/DAT obtained by rheology at T_{ref} = 333 K (figure S8 in section IV of the S. I.). The lines are the fits to the data using the VFTH equation, except the data for MWS for PPO-UPY and $\nu_{d,PEO-upy}$ where the Arrhenius equation was used. The colours of the lines are the same as the symbols. The respective fit parameters are present in Table 3 and Table 4.

The network detachment relaxation time for PPO-UPY ($\tau_{d,PPO-UPY}$) resulting from the viscosity data is much faster than the corresponding network detachment relaxation time obtained in similar

conditions for PEO-UPY ($\tau_{\mathrm{d,PEO-UPY}}$) viscosity data.[18] **Table 4** presents the fit parameters from the Arrhenius equation fit to the MWS, $\tau_{\mathrm{d,PPO-UPY}}$ and $\tau_{\mathrm{d,PEO-UPY}}$. The relaxation time at infinite temperature, τ_0 for PEO-UPY is higher than for PPO-UPY as observed in **Figure 10**. This also illustrates the minor impact of the activation energy of the UPY end group association in the dynamics, which is relatively similar in both PEO and PPO and thus cannot be taken as a reason for the large difference in the times for these process between both poly(alkyl ether) supramolecular chains. In fact, this seems to be in accordance to the typical energy barrier specifically imposed by the hydrogen bonds ($10-65\ \mathrm{kJ\cdot mol^{-1}}$) found in literature.[54] This fact suggests the good assignment of the relaxation times. A higher value of the activation would seem to indicate that not only the H-bonding groups dynamics would be involved but also the chain dynamics.

Table 4. Fitting parameters of the temperature dependence of the network detachment relaxation time, τ_{d} for both PPO-UPY and PEO-UPY, as well of the MWS for PPO-UPY.[54]

		E_{a} [kJ·mol^{-1}]	τ_0 [ns]
MWS	PPO-UPY	39±3	(3.5±2) × 10^{1}
τ_{d}	PPO-UPY	~55	~6.4× 10^{-1}
	PEO-UPY	43±4	(2.1±1) × 10^{4}

4. CONCLUSION

In this work we studied melts of supramolecular PPO polymers with different H- bonding end groups (THY/DAT and UPY) by means of scattering, rheology, dielectric spectroscopy and calorimetry; the PPO backbone polymer chains are shorter than the entanglement length. Both

structure and dynamics are compared with work published recently[18] for identically short supramolecular PEO polymer chains functionalized with the same H-bonding end groups.

Relatively to the structure, PPO-THY/DAT associates in linear chains as judged by small angle scattering analysis. However, PPO-THY/DAT forms longer chains than PEO-THY/DAT, revealing the influence of the backbone main chain polarity on this H-bonding end groups association. Moreover, PPO-UPY as PEO-UPY, presents spherical-like phase segregated cluster morphology, but for PPO-UPY, two very different types of bonds are formed by the same species of end groups establishing a dual network behavior: (i) a part of transient bonds releases stress by a transient network mechanism controlled by the characteristic times of association/dissociation between pairs of end groups involving most probably just two chain ends. This part is perceived by the similar dielectric spectra in comparison with PPO and (ii) some much more stable type of bond or associate that forms the UPY clusters, which requires elevated temperatures to be dissociated as judged by mechanical analysis.

Concerning the dynamics, the combination of the experimental methods allows to distinguish between both the segmental and chain dynamics as well as the lifetimes of the H-bonding groups in the associated chains and network for the different supramolecular poly(alkyl ether) chains. Particularly, the temperature dependence of the association/dissociation lifetimes for both PPO and PEO possessing THY/DAT H-bonding groups at the ends, emerge as independent of the poly(alkyl ether) main chain polarity. This is not the case for the UPY end groups. The network detachment times are higher and the segmental dynamics is much slower for PEO-UPY than for PPO-UPY. This points to the fact that the temperature dependence of the association/dissociation times of UPY groups in the clusters are dependent on the polarity of the poly(alkyl ether) chain,

that seem to play a fundamental role in defining the time scale of the dissociation process for these supramolecular polymers.

ASSOCIATED CONTENT

Supporting Information. The Supporting Information is available free of charge on the ACS Publications website.

Supramolecular polymer synthesis and characterization (figures S1 to S5), theories used in the scattering characterization (equations S1 to S22) including the Flory-Huggins interaction parameter χ (equation S23) and rheology data (figures S6 to S8 and tables S1 to S3) and dielectric relaxation spectroscopy data (figure S9 and tables S4 to S8).

AUTHOR INFORMATION

Corresponding Author

* Author to whom correspondence should be addressed: ana.eliasbras@uni-koeln.de; Tel.: +49-221-470-5473

Notes

The authors declare no competing financial interest.

Present Addresses

†If an author's address is different than the one given in the affiliation line, this information may be included here.

Author Contributions

The manuscript was written through contributions of all authors. All authors have given approval to the final version of the manuscript.

Funding Sources

A. R. Brás would like to acknowledge the German Research Foundation (DFG) for grant number BR 5301 / 1 and the QM² at University of Cologne for funding.

ACKNOWLEDGMENT

A. Brás would like to acknowledge the German Research Foundation (DFG) for grant number BR 5301 / 1 and the QM² at University of Cologne for funding. The authors would like to thank Prof. D. Richter for the scientific discussions and Dr. Reiner Zorn for the help accessing the BDS facilities at the Forschungszentrum Jülich.

REFERENCES

(1) Zhang, Q.; Weber, C.; Schubert, U. S.; Hoogenboom, R. Thermoresponsive Polymers with Lower Critical Solution Temperature: From Fundamental Aspects and Measuring Techniques to Recommended Turbidimetry Conditions. *Mater. Horizons* **2017**, *4* (2), 109–116. https://doi.org/10.1039/c7mh00016b.

(2) Seiffert, S.; Sprakel, J. Physical Chemistry of Supramolecular Polymer Networks. *Chem. Soc. Rev.* **2012**, *41*, 909–930. https://doi.org/10.1039/c1cs15191f.

(3) *Supramolecular Polymer Networks and Gels*; Seiffert, S., Ed.; Springer: Berlin, Heidelberg,

Germany, 2015; Vol. 268. https://doi.org/10.1016/j.carbpol.2014.04.040.

(4) Peterlik, H.; Binder, W. H.; Diana, D. A Dual Crosslinked Self-Healing System : Supramolecular and Covalent Network Formation of Four-Arm Star Polymers. **2015**, *69*, 264–273. https://doi.org/10.1016/j.polymer.2015.01.073.

(5) Herbst, F.; Döhler, D.; Michael, P.; Binder, W. H. Self-Healing Polymers via Supramolecular Forces. *Macromol. Rapid Commun.* **2013**, *34* (3), 203–220. https://doi.org/10.1002/marc.201200675.

(6) *Hydrogen Bonded Polymers*, 207th ed.; Binder, W., Ed.; Springer-Verlag Berlin Heidelberg, 2007. https://doi.org/10.1038/216619a0.

(7) Stukalin, E. B.; Cai, L.; Kumar, N. A.; Leibler, L.; Rubinstein, M. Self-Healing of Unentangled Polymer Networks with Reversible Bonds. *Macromolecules* **2013**, *46* (18), 7525–7541. https://doi.org//10.1021/ma401111n.

(8) Cortese, J.; Soulié-Ziakovic, C.; Cloitre, M.; Tencé-Girault, S.; Leibler, L. Order-Disorder Transition in Supramolecular Polymers. *J. Am. Chem. Soc.* **2011**, *133* (49), 19672–19675. https://doi.org/10.1021/ja209126a.

(9) Herbst, F.; Schröter, K.; Gunkel, I.; Gröger, S.; Thurn-Albrecht, T.; Balbach, J.; Binder, W. H. Aggregation and Chain Dynamics in Supramolecular Polymers by Dynamic Rheology: Cluster Formation and Self-Aggregation. *Macromolecules* **2010**, *43* (23), 10006–10016. https://doi.org/10.1021/ma101962y.

(10) Stadler, F. J.; Pyckhout-Hintzen, W.; Schumers, J. M.; Fustin, C. A.; Gohy, J. F.; Bailly, C. Linear Viscoelastic Rheology of Moderately Entangled Telechelic Polybutadiene

Temporary Networks. *Macromolecules* **2009**, *42* (16), 6181–6192. https://doi.org/10.1021/ma802488a.

(11) Lange, R. F. M.; Gurp, M. V. A. N.; Meijer, E. W. Hydrogen-Bonded Supramolecular Polymer Networks. *J. Polym. Sci. Part A Polym. Chem.* **1999**, *37*, 3657–3670. https://doi.org/CCC 0887-624X/99/193657-14.

(12) Xing, K.; Tress, M.; Cao, P. F.; Fan, F.; Cheng, S.; Saito, T.; Sokolov, A. P. The Role of Chain-End Association Lifetime in Segmental and Chain Dynamics of Telechelic Polymers. *Macromolecules* **2018**, *51* (21), 8561–8573. https://doi.org/10.1021/acs.macromol.8b01210.

(13) Yan, T.; Schröter, K.; Herbst, F.; Binder, W. H.; Thurn-Albrecht, T. Unveiling the Molecular Mechanism of Self-Healing in a Telechelic, Supramolecular Polymer Network. *Sci. Rep.* **2016**, *6* (September), 1–8. https://doi.org/10.1038/srep32356.

(14) Chen, S.; Binder, W. H. Dynamic Ordering and Phase Segregation in Hydrogen-Bonded Polymers. *Acc. Chem. Res.* **2016**, *49* (7), 1409–1420. https://doi.org/10.1021/acs.accounts.6b00174.

(15) Müller, M.; Seidel, U.; Stadler, R. Influence of Hydrogen Bonding on the Viscoelastic Properties of Thermoreversible Networks: Analysis of the Local Complex Dynamics. *Polymer (Guildf).* **1995**, *36* (16), 3143–3150. https://doi.org/10.1016/0032-3861(95)97877-I.

(16) Jangizehi, A.; Ahmadi, M.; Seiffert, S. Emergence, Evidence, and Effect of Junction Clustering in Supramolecular Polymer Materials. *Mater. Adv.* **2021**, *2* (5), 1425–1453.

https://doi.org/10.1039/d0ma00795a.

(17) Xing, K.; Tress, M.; Cao, P.; Cheng, S.; Saito, T.; Novikov, V. N.; Sokolov, A. P. Hydrogen-Bond Strength Changes Network Dynamics in Associating Telechelic PDMS. *Soft Matter* **2018**, *14* (7), 1235–1246. https://doi.org/10.1039/c7sm01805c.

(18) Brás, A.; Arizaga, A.; Agirre, U.; Dorau, M.; Houston, J.; Radulescu, A.; Kruteva, M.; Pyckhout-Hintzen, W.; Schmidt, A. M. Chain-End Effects on Supramolecular Poly(Ethylene Glycol) Polymers. *Polymers (Basel)*. **2021**, *13* (14), 2235. https://doi.org/10.3390/polym13142235.

(19) Yan, T.; Schröter, K.; Herbst, F.; Binder, W. H.; Thurn-Albrecht, T. What Controls the Structure and the Linear and Nonlinear Rheological Properties of Dense, Dynamic Supramolecular Polymer Networks? *Macromolecules* **2017**, *50* (7), 2973–2985. https://doi.org/10.1021/acs.macromol.6b02507.

(20) Herbst, F.; Binder, W. H. Comparing Solution and Melt-State Association of Hydrogen Bonds in Supramolecular Polymers. *Polym. Chem.* **2013**, *4* (12), 3602–3609. https://doi.org/10.1039/c3py00362k.

(21) Gainaru, C.; Hecksher, T.; Fan, F.; Xing, K.; Cetinkaya, B.; Olsen, N. B.; Dyre, J. C.; Sokolov, A. P.; Böhmer, R. Simple-Liquid Dynamics Emerging in the Mechanical Shear Spectra of Poly(Propylene Glycol). *Colloid Polym. Sci.* **2017**, *295* (12), 2433–2437. https://doi.org/10.1007/s00396-017-4206-6.

(22) Venkatramanan, K.; Arumugam, V. Viscosity Studies on Polypropylene Glycol and Its Blend. *Int. J. Thermophys.* **2006**, *27* (1), 66–78. https://doi.org/10.1007/s10765-006-0021-

x.

(23) Heinrich, G.; Alig, I.; Donth, E. A Model for the Onset of Entanglements of Transient Hydrogen-Bonded Intermolecular Structures in Oligomeric Poly(Propylene Glycol). *Polymer (Guildf)*. **1988**, *29* (7), 1198–1202. https://doi.org/10.1016/0032-3861(88)90044-4.

(24) Wang, C. H.; Fytas, G.; Lilge, D.; Dorfmüller, T. H. Laser Light Beating Spectroscopic Studies of Dynamics in Bulk Polymers: Polypropylene Glycol). *Macromolecules* **1981**, *14* (5), 1363–1370. https://doi.org/10.1021/ma50006a042.

(25) Ol'khovikov, O. A.; Golubev, V. M.; Gladkovskii, G. A. The Viscosity of Polypropylene Glycol Oligomers as a Function of Temperature and Molecular Weight. *Polym. Sci. U.S.S.R.* **1973**, *15* (11), 2843–2849. https://doi.org/10.1016/0032-3950(73)90343-2.

(26) Schönhals, A.; Stauga, R. Broadband Dielectric Study of Anomalous Diffusion in a Poly(Propylene Glycol) Melt Confined to Nanopores. *J. Chem. Phys.* **1998**, *108* (12), 5130–5136. https://doi.org/10.1063/1.475918.

(27) Gainaru, C.; Hiller, W.; Böhmer, R. A Dielectric Study of Oligo- and Poly(Propylene Glycol). *Macromolecules* **2010**, *43* (4), 1907–1914. https://doi.org/10.1021/ma9026383.

(28) Plazek, D. J.; Schlosser, E.; Schönhals, A.; Ngai, K. L. Breakdown of the Rouse Model for Polymers near the Glass Transition Temperature. *J. Chem. Phys.* **1993**, *98* (8), 6488–6491.

(29) Brás, A. R.; Hövelmann, C. H.; Antonius, W.; Teixeira, J.; Radulescu, A.; Allgaier, J.; Pyckhout-Hintzen, W.; Wischnewski, A.; Richter, D. Molecular Approach to Supramolecular Polymer Assembly by Small Angle Neutron Scattering. *Macromolecules*

2013, *46* (23), 9446–9454. https://doi.org/10.1021/ma401714r.

(30) Krutyeva, M.; Brás, A. R.; Antonius, W.; Hövelmann, C. H.; Poulos, A. S.; Allgaier, J.; Radulescu, A.; Lindner, P.; Pyckhout-Hintzen, W.; Wischnewski, A.; Richter, D. Association Behavior, Diffusion, and Viscosity of End-Functionalized Supramolecular Poly(Ethylene Glycol) in the Melt State. *Macromolecules* **2015**, *48* (24), 8933–8946. https://doi.org/10.1021/acs.macromol.5b02060.

(31) Söntjens, S. H. M.; Sijbesma, R. P.; Van Genderen, M. H. P.; Meijer, E. W. Stability and Lifetime of Quadruply Hydrogen Bonded 2-Ureido-4[1H]-Pyrimidinone Dimers. *J. Am. Chem. Soc.* **2000**, *122* (31), 7487–7493. https://doi.org/10.1021/ja000435m.

(32) Folmer, B. J. B.; Sijbesma, R. P.; Versteegen, R. M.; van der Rijt, J. A. J.; Meijer, E. W. Supramolecular Polymer Materials: Chain Extension of Telechelic Polymers Using a Reactive Hydrogen-Bonding Synthon. *Adv. Mater.* **2000**, *12* (12), 874–878. https://doi.org/10.1002/1521-4095(200006)12:12<874.

(33) Kentzinger, E.; Krutyeva, M.; Rücker, U. GALAXI: Gallium Anode Low-Angle x-Ray Instrument. *J. large-scale Res. Facil. JLSRF* **2016**, *2*, 1–5. https://doi.org/10.17815/jlsrf-2-109.

(34) Viciosa, M. T. Molecular Mobility of N-Ethylene Glycol Dimethacrylate Glass Formers upon Free Radical Polymerization, Faculdade de Ciencias e Tecnologia da Universidade Nova de Lisboa, Portugal, 2007.

(35) Turnhout, J. Van; Michael, W. Analysis of Complex Dielectric Spectra . I . One-Dimensional Derivative Techniques and Three-Dimensional Modelling. *J. Non. Cryst.*

Solids **2002**, *305*, 40–49.

(36) Hammouda, B. *Probing Nanoscale Structures – The SANS Toolbox*; National Institute of Standards and Technology Center: Gaithersburg, 2016. https://doi.org/10.1016/j.nano.2007.10.035.

(37) Niedzwiedz, K.; Wischnewski, A.; Pyckhout-Hintzen, W.; Allgaier, J.; Richter, D.; Faraone, A. Chain Dynamics and Viscoelastic Properties of Poly(Ethylene Oxide). *Macromolecules* **2008**, *41* (13), 4866–4872. https://doi.org/10.1021/ma800446n.

(38) Hammouda, B.; Ho, D.; Kline, S. SANS from Poly(Ethylene Oxide)/Water Systems. *Macromolecules* **2002**, *35* (22), 8578–8585. https://doi.org/10.1021/ma011657n.

(39) Gerstl, C.; Schneider, G. J.; Pyckhout-Hintzen, W.; Allgaier, J.; Richter, D.; Alegría, A.; Colmenero, J. Segmental and Normal Mode Relaxation of Poly(Alkylene Oxide)s Studied by Dielectric Spectroscopy and Rheology. *Macromolecules* **2010**, *43* (11), 4968–4977. https://doi.org/10.1021/ma100384j.

(40) Hammouda, B. SANS from Polymers-Review of the Recent Literature. *Polym. Rev.* **2010**, *50* (1), 14–39. https://doi.org/10.1080/15583720903503460.

(41) Hammouda, B. *A Tutorial on Small-Angle Neutron Scattering From Polymers*; National Institute of Standards and Technology: Gaithersburg, 1995.

(42) Staropoli, M.; Raba, A.; Hövelmann, C. H.; Krutyeva, M.; Allgaier, J.; Appavou, M. S.; Keiderling, U.; Stadler, F. J.; Pyckhout-Hintzen, W.; Wischnewski, A.; Richter, D. Hydrogen Bonding in a Reversible Comb Polymer Architecture: A Microscopic and Macroscopic Investigation. *Macromolecules* **2016**, *49* (15), 5692–5703.

https://doi.org/10.1021/acs.macromol.6b00978.

(43) Vonk, C. G. Investigation of Non-Ideal Two-Phase Polymer Structures by Small-Angle X-Ray Scattering. *J. Appl. Crystallogr.* **1973**, *6* (2), 81–86. https://doi.org/10.1107/s0021889873008204.

(44) Gerstl, C.; Schneider, G. J.; Pyckhout-Hintzen, W.; Allgaier, J.; Willbold, S.; Hofmann, D.; Disko, U.; Frielinghaus, H.; Richter, D. Chain Conformation of Poly(Alkylene Oxide)s Studied by Small-Angle Neutron Scattering. *Macromolecules* **2011**, *44* (15), 6077–6084. https://doi.org/10.1021/ma201288a.

(45) Jansson, J.; Schillén, K.; Nilsson, M.; Söderman, O.; Fritz, G.; Bergmann, A.; Glatter, O. Small-Angle X-Ray Scattering, Light Scattering, and NMR Study of PEO-PPO-PEO Triblock Copolymer/Cationic Surfactant Complexes in Aqueous Solution. *J. Phys. Chem. B* **2005**, *109* (15), 7073–7083. https://doi.org/10.1021/jp0468354.

(46) Cortese, J. Organizations in Supramolecular Polymers: From the Solution to the Bulk Behavior, Université Pierre et Marie Curie - Paris VI, France, 2013.

(47) Yan, T.; Schröter, K.; Herbst, F.; Binder, W. H.; Thurn-Albrecht, T. Nanostructure and Rheology of Hydrogen-Bonding Telechelic Polymers in the Melt: From Micellar Liquids and Solids to Supramolecular Gels. *Macromolecules* **2014**, *47* (6), 2122–2130. https://doi.org/10.1021/ma402007f.

(48) Frielinghaus, H.; Pyckhout-Hintzen, W. *Neutron Scattering on Different States of Polymer-Clay Compounds: From Solution to Dry States*; Elsevier Inc.: Amsterdam, Netherlands, 2017. https://doi.org/10.1016/B978-0-323-46153-5.00010-0.

(49) Hammouda, B.; Ho, D. L.; Kline, S. Insight into Clustering in Poly(Ethylene Oxide) Solutions. *Macromolecules* **2004**, *37* (18), 6932–6937. https://doi.org/10.1021/ma049623d.

(50) Slawecki, T. M.; Glinka, C. J.; Hammouda, B. Shear-Induced Micellar Crystal Structures in an Aqueous Triblock Copolymer Solution. *Phys. Rev. E - Stat. Physics, Plasmas, Fluids, Relat. Interdiscip. Top.* **1998**, *58* (4), R4084–R4087. https://doi.org/10.1103/PhysRevE.58.R4084.

(51) Jouault, N.; Kumar, S. K.; Smalley, R. J.; Chi, C.; Moneta, R.; Wood, B.; Salerno, H.; Melnichenko, Y. B.; He, L.; Guise, W. E.; Hammouda, B.; Crawford, M. K. Do Very Small POSS Nanoparticles Perturb S-PMMA Chain Conformations? *Macromolecules* **2018**, *51* (14), 5278–5293. https://doi.org/10.1021/acs.macromol.8b00432.

(52) Bartlett, P.; Ottewill, R. H. A Neutron Scattering Study of the Structure of a Bimodal Colloidal Crystal. *J. Chem. Phys.* **1992**, *96* (4), 3306–3318. https://doi.org/10.1063/1.461926.

(53) Royall, C. P.; Poon, W. C. K.; Weeks, E. R. In Search of Colloidal Hard Spheres. *Soft Matter* **2013**, *9* (1), 17–27. https://doi.org/10.1039/c2sm26245b.

(54) Monkenbusch, M.; Krutyeva, M.; Pyckhout-Hintzen, W.; Antonius, W.; Hövelmann, C. H.; Allgaier, J.; Brás, A.; Farago, B.; Wischnewski, A.; Richter, D. Molecular View on Supramolecular Chain and Association Dynamics. *Phys. Rev. Lett.* **2016**, *117* (14), 1–5. https://doi.org/10.1103/PhysRevLett.117.147802.

(55) Lou, N.; Wang, Y.; Li, H.; Sokolov, A. P.; Xiong, H. Glassy Dynamics of Hydrogen-Bonded Heteroditopic Molecules. *Polymer (Guildf).* **2012**, *53* (20), 4455–4460.

https://doi.org/10.1016/j.polymer.2012.07.052.

(56) Tress, M.; Xing, K.; Ge, S.; Cao, P.; Saito, T.; Sokolov, A. What Dielectric Spectroscopy Can Tell Us about Supramolecular Networks. *Eur. Phys. J. E* **2019**, *42* (10), 133. https://doi.org/10.1140/epje/i2019-11897-4.

(57) Richter, D.; Monkenbusch, M.; Willner, L.; Wischnewski, A.; Arbe, A.; Colmenero, J. Experimental Aspects of Polymer Dynamics. *Polym. Int.* **2002**, *1218* (52), 1211–1218. https://doi.org/10.1002/pi.908.

(58) Likhtman, A. E. Viscoelasticity and Molecular Rheology. *Polym. Sci. A Compr. Ref.* **2012**, *1*, 133–179. https://doi.org/10.1016/B978-0-444-53349-4.00008-X.

(59) Padding, J. T. *Theory of Polymer Dynamics*; University of Cambridge, 2005.

(60) James, N. M.; Han, E.; de la Cruz, R. A. L.; Jureller, J.; Jaeger, H. M. Interparticle Hydrogen Bonding Can Elicit Shear Jamming in Dense Suspensions. *Nat. Mater.* **2018**, *17* (11), 965–970. https://doi.org/10.1038/s41563-018-0175-5.

(61) Tripathi, A.; Tam, K. C.; McKinley, G. H. Rheology and Dynamics of Associative Polymers in Shear and Extension: Theory and Experiments. *Macromolecules* **2006**, *39* (5), 1981–1999. https://doi.org/10.1021/ma051614x.

(62) Ma, S. X.; Cooper, S. L. Shear Thickening in Aqueous Solutions of Hydrocarbon End-Capped Poly(Ethylene Oxide). *Macromolecules* **2001**, *34* (10), 3294–3301. https://doi.org/10.1021/ma001772i.

(63) Lei, Y.; Lodge, T. P. Effects of Component Molecular Weight on the Viscoelastic Properties

of Thermoreversible Supramolecular Ion Gels via Hydrogen Bonding. *Soft Matter* **2012**, *8* (7), 2110–2120. https://doi.org/10.1039/c2sm06652a.

(64) Marrucci, G.; Bhargava, S.; Cooper, S. L. Models of Shear-Thickening Behavior in Physically Cross-Linked Networks. *Macromolecules* **1993**, *26* (24), 6483–6488. https://doi.org/10.1021/ma00076a027.

(65) Koga, T.; Tanaka, F.; Motokawa, R.; Koizumi, S. Theoretical Modeling of Associated Structures in Aqueous Solutions of Hydrophobically Modified Telechelic PNIPAM Based on a Neutron Scattering Study. **2008**, 9413–9422.

(66) Jiang, B.; Keffer, D. J.; Edwards, B. J.; Allred, J. N. Modeling Shear Thickening in Dilute Polymer Solutions: Temperature, Concentration, and Molecular Weight Dependencies. *J. Appl. Polym. Sci.* **2003**, *90* (11), 2997–3011. https://doi.org/10.1002/app.12950.

(67) Richter, D.; Monkenbusch, M.; Allgeier, J.; Arbe, A.; Colmenero, J.; Farago, B.; Cheol Bae, Y.; Faust, R. From Rouse Dynamics to Local Relaxation: A Neutron Spin Echo Study on Polyisobutylene Melts. *J. Chem. Phys.* **1999**, *111* (13), 6107–6120. https://doi.org/10.1063/1.479907.

(68) Krutyeva, M.; Martin, J.; Arbe, A.; Colmenero, J.; Mijangos, C.; Schneider, G. J.; Unruh, T.; Su, Y.; Richter, D. Neutron Scattering Study of the Dynamics of a Polymer Melt under Nanoscopic Confinement. *J. Chem. Phys.* **2009**, *131* (17), 174901. https://doi.org/10.1063/1.3258329.

(69) Fetters, L. J.; Lohse, D. J.; Richter, D.; Witten, T. A.; Zirkel, A. Connection between Polymer Molecular Weight, Density, Chain Dimensions, and Melt Viscoelastic Properties.

Macromolecules **1994**, *27* (17), 4639–4647. https://doi.org/10.1021/ma00095a001.

(70) Richter, D.; Willner, L.; Zirkel, A.; Farago, B.; Fetters, L. J.; Huang, J. S. Polymer Motion at the Crossover from Rouse to Reptation Dynamics. *Macromolecules* **1994**, *27* (25), 7437–7446. https://doi.org/10.1021/ma00103a029.

(71) Xu, D.; Hawk, J. L.; Loveless, D. M.; Jeon, S. L.; Craig, S. L. Mechanism of Shear Thickening in Reversibly Cross-Linked Supramolecular Polymer Networks. *Macromolecules* **2010**, *43* (7), 3556–3565. https://doi.org/10.1021/ma100093b.

(72) Kharel, A.; Lodge, T. P. Effect of Ionic Liquid Components on the Coil Dimensions of PEO. *Macromolecules* **2019**, *52* (8), 3123–3130. https://doi.org/10.1021/acs.macromol.9b00354.

(73) *Broadband Dielectric Spectroscopy*; Kremer, F., Schönhals, A., Eds.; Springer: Berlin, Heidelberg, Germany, 2003.

(74) Williams, G. Molecular Aspects of Multiple Dielectric Relaxation Processes in Solid Polymers. In *Multiple Dielectric Relaxation Processes*; W. Kern, Ed.; 1979; pp 60–92.

(75) Casalini, R.; Roland, C. M. Temperature and Density Effects on the Local Segmental and Global Chain Dynamics of Poly(Oxybutylene). *Macromolecules* **2005**, *38* (5), 1779–1788. https://doi.org/10.1021/ma0476902.

(76) Schönhals, A.; Schlosser, E. Relationship between Segmental and Chain Dynamics in Polymer Melts as Studied by Dielectric Spectroscopy. *Phys. Scr.* **1993**, *1993* (T49A), 233–236. https://doi.org/10.1088/0031-8949/1993/T49A/039.

(77) Lovell, R. Application of Kramers-Kronig Relations to the Interpretation of Dielectric Data. *J. Phys. C Solid State Phys.* **1974**, *7* (2), 4378–4384.

(78) Roland, C. M.; Casalini, R. Temperature Dependence of Local Segmental Motion in Polystyrene and Its Variation with Molecular Weight. **2003**, *119* (3). https://doi.org/10.1063/1.1581850.

(79) Schlosser, E.; Schönhals, A. Relation between Main- and Normal-Mode Relaxation. A Dielectric Study on Poly(Propyleneoxide). *Prog. Colloid Polym. Sci.* **1993**, *91* (1993), 158–161. https://doi.org/10.1007/bfb0116484.

(80) Goldansaz, H.; Fustin, C. A.; Wübbenhorst, M.; Van Ruymbeke, E. How Supramolecular Assemblies Control Dynamics of Associative Polymers: Toward a General Picture. *Macromolecules* **2016**, *49* (5), 1890–1902. https://doi.org/10.1021/acs.macromol.5b01535.

(81) Lou, N.; Wang, Y.; Li, X.; Li, H.; Wang, P.; Wesdemiotis, C.; Sokolov, A. P.; Xiong, H. Dielectric Relaxation and Rheological Behavior of Supramolecular Polymeric Liquid. *Macromolecules* **2013**, *46* (8), 3160–3166. https://doi.org/10.1021/ma400088w.

(82) Reiser, A.; Kasper, G.; Gainaru, C.; Böhmer, R. Communications : High-Pressure Dielectric Scaling Study of a Monohydroxy Alcohol. *J. Chem. Phys.* **2010**, *132* (May), 181101. https://doi.org/10.1063/1.3421555.

(83) Peterson, J. D.; Cates, M. E. A Full-Chain Tube-Based Constitutive Model for Living Linear Polymers. *J. Rheol. (N. Y. N. Y).* **2020**, *64* (6), 1465–1496. https://doi.org/10.1122/8.0000114.

(84) Huth, H.; Beiner, M.; Donth, E. Temperature Dependence of Glass-Transition

Cooperativity from Heat-Capacity Spectroscopy : Two Post-Adam-Gibbs Variants. *Phys. Rev. B* **2000**, *61* (22), 92–101.

(85) Ngai, K. L. Correlation between -Relaxation and R -Relaxation in the Family of Poly (n -Butyl Methacrylate- Stat -Styrene) Random Copolymers. *Macromolecules* **1999**, *32* (21), 7140–7146.

(86) Buchenau, U. Glass Transition. In *Scattering Methods for Condensed Matter Research: Towards Novel Applications at Future Sources Lecture*; Angst, M., Brückel, T., Richter, D., Zorn, R., Eds.; Forschungszentrum Jülich GmbH, 2012; Vol. 33.